A search for galaxies producing CIV absorption in QSO spectra

Jean Marc Schwartzenberg

A SEARCH FOR GALAXIES PRODUCING CIV ABSORPTION IN QSO SPECTRA

by
Jean Marc Schwartzenberg

January 1993

A thesis submitted to the University of Durham in accordance with the regulations for admission to the degree of Master of Science.

ABSTRACT

This thesis describes an infrared search for the intervening galaxies responsible for some of the heavy-element absorption lines observed in QSO spectra. Deep K-band images have been obtained of 11 QSOs whose spectra are known to contain multiple C IV absorption systems in the redshift range $1.2 \leq z \leq 2.0$. After background subtraction, a clear excess of sources is detected within a small angular separation ($\approx 6.''0$) of the QSOs. We discuss the possible origins of this excess, in particular the hypotheses that the excess arises from QSO-galaxy associations or from Mg II systems at lower redshifts, but consider them unlikely in the light of previous studies. We thus conclude that the excess objects are most likely to be associated with the C IV absorption systems.

From a final sample of 19 candidate absorbers with a mean redshift $\overline{z} = 1.6$, we find that the absorbing candidate population consists of bright L^* galaxies whose luminosities are similar to their present-day counterparts. Their linear impact parameters ($30{-}40h_{50}^{-1}$ kpc) are found to be similar to those of spectroscopically-confirmed Mg II absorbers at lower redshifts, ruling out significant evolution in galactic halo sizes from $z \simeq 1.6$ to $z \simeq 0.5$. Optical R and I-band photometry of four fields is also presented, allowing us to determine optical-infrared colours for a subsample of our candidates; these are found to be typical of late-type, star-forming galaxies. We thus find that our candidate absorbers share several properties with the galaxies known to give rise to lower redshift Mg II absorption lines.

PREFACE

The work presented in this thesis was carried out between October 1991 and December 1992, while the author was a student in the Department of Physics, under the supervision of Professor R.S. Ellis. No part of this work has been submitted for any other degree in this or in any other University.

Part of this work has been carried out in collaboration with Professor R.S. Ellis and Dr. A. Aragón-Salamanca.

CONTENTS

1 INTRODUCTION

1.1 OVERVIEW

Our understanding of the Universe has changed dramatically in the last 70 years, since Edwin Hubble first realised that the diffuse clouds observed in the deep sky were in fact galaxies like our own, each consisting of billions of stars. Since this fundamental discovery, much ground has been broken and our knowledge has considerably evolved. It is now widely believed that the Universe formed in a large explosion of matter from a singularity in spacetime, and that, as a consequence of this initial explosion or *Big Bang*, the Universe is still expanding. This idea was prompted by the discovery, again by Hubble, that all galaxies are receding from each other. One of the most direct tools for understanding the Universe are therefore galaxies, as most of the matter present or believed to be present in the Universe is associated with them in one way or another.

This thesis describes a project undertaken to identify and study normal galaxies at large lookback times. By understanding their evolutionary behaviour over a period of time comparable to the age of the Universe itself, we might hope to obtain the answers to some fundamental questions concerning the galaxies' formation and evolution, and ultimately

reach a better understanding of the physical conditions prevailing in the Universe we live in.

1.2 GALAXY EVOLUTION

Several factors bear an influence on the properties of a galaxy after its formation and collapse. The simple ageing of the stellar populations, referred to as *passive evolution*, will have effects on a galaxy's luminosity, colours and spectral features. These are also affected by other factors such as episodic star formation, dynamical interactions and galaxy-galaxy mergers. In particular, there is now considerable evidence that the environment plays an important role in a galaxy's evolution (e.g. Zepf 1991, Oemler 1992, Allington-Smith *et al.* 1992). In this section we present a brief review of the present knowledge of galaxy evolution, from the first models of spectral synthesis to the most recent deep number counts and their implications.

1.2.1 Evolution of Field Galaxies

The detection of normal galaxies at high redshift has only become a reality in the last 10-15 years, with the first deep photographic surveys of faint galaxies. However, it was known long before these surveys that galaxies had to evolve, since they consist of ordinary stars, and that these stars have a finite lifetime during which their properties change. The detailed study of this evolution was pioneered by B. M. Tinsley, who first quantified the effect of stellar evolution on the spectrum of a galaxy at different redshifts. The method assigns initial parameters to a galaxy (Initial Mass Function, Star Formation

Rate) which determine the mass of the forming stars. The stars are then evolved along evolutionary tracks and the galaxy's spectrum is thus predicted at different epochs. The method is known as *evolutionary synthesis* and is reviewed by Tinsley (1980). Despite a considerable dependence on several uncertain parameters, most of which are related to the poorly understood late stages of stellar evolution, this approach is still followed today – some recent examples are Bruzual & Charlot (1992), Guiderdoni & Rocca-Volmerange (1990), Buzzoni (1989).

The late 1970's saw the appearance of the first photographic surveys of large numbers of faint galaxies (e.g. Kron 1978, Tyson & Jarvis 1979, Peterson *et al.* 1979). These surveys, in the form of number-magnitude counts, all agreed in two fundamental points: they were consistently detecting larger numbers of galaxies than expected, irrespective of the cosmological model used, and the populations showed a strong blueward trend at fainter magnitudes. The development of CCD detectors has pushed the number-magnitude counts to much fainter limits – the most recent reach $B = 28$ (Metcalfe *et al.* 1991), $R = 26.5$ (Tyson 1988a), $I = 24$ (Tyson 1988a), $K = 23$ (Cowie *et al.* 1991a) – but has not altered this scenario, the numbers still being higher than any prediction. The initial interpretation of the blue excess was simply that galaxies were bluer and more luminous in the past, perhaps due to an enhanced star-formation rate (e.g. Ellis 1982).

An important step towards understanding the faint galaxy counts would be to measure the galaxies' redshifts, so as to obtain their spatial distribution. Additionally, spectral features would provide an important source of information on properties such as their star formation rates. Due to the long exposure times needed to secure galaxy redshifts at faint limits, spectroscopy of large numbers of faint galaxies was limited until the first multi-object spectrographs were made available (Ellis & Parry 1987). The most

important faint-galaxy redshift surveys to date are those of Broadhurst *et al.* (1988), Colless *et al.* (1990) and Lilly *et al.* (1991). The two principal results that emerged from these spectroscopic surveys were that the redshift distribution of the galaxies observed was consistent with no luminosity evolution, contrary to the simple models explaining the number-magnitude relation, and that a large fraction of galaxies showed evidence for strong star formation. Since luminosity evolution alone could not be responsible for the excess of faint blue galaxies, the authors suggested that the steep slope in the number-magnitude relation was due to low luminosity galaxies undergoing bursts of star formation at moderate redshifts and thus dominating the field counts.

Several models have surfaced in recent years which attempt to accommodate the results of the spectral surveys and the number-magnitude counts. Clearly the $n(z)$ and $n(m)$ results require a change in the number density of galaxies of a given luminosity between $z \simeq 0.5$ and the present epoch, rather than just a change in the characteristic luminosity. The most accepted models are the merging models of, e.g., Broadhurst *et al.* (1992), Lilly *et al.* (1991) or Koo (1990), who suggest that a much larger number of galaxies existed in the past, which have merged to form the massive present-day systems. This so-called "merging hypothesis" at present appears to be the most likely explanation to the faint blue counts problem.

An alternative model has been proposed by Cowie *et al.* (1991b), whereby an additional population of dwarf ellipticals formed and underwent their first starbursts at $z \approx 0.4$. Subsequent gas loss would then have inhibited further star formation, causing the majority of this population to fade beyond detection. A theoretical justification for this model has been attempted by Babul & Rees (1992), although the implied redshift of formation and starburst is considerably higher at $z \simeq 1.0 - 1.5$.

All the models outlined above have attempted to explain the galaxy number counts in terms of astrophysical events. However, another important factor to consider when interpreting the results is the cosmological model used. Although the blue counts show an excess over the predictions of any geometry (whether an open, flat or closed Universe is assumed), the most direct cosmological interpretation is that they favour a low-density, open Universe, as this would then provide more volume to accommodate the large number of galaxies observed (Guiderdoni 1991). However, the difficulty in accepting this simple hypothesis is perhaps in part due to the highly successful theory of inflation (see Guth 1991 for a recent review), which requires $\Omega_0 = 1$. Indeed inflation has been so elegant at explaining many cosmological phenomena that its appeal is becoming more widespread and thus any model requiring $\Omega_0 \neq 1$ tends to encounter heavy resistance.

The optical number counts could still be better reconciled with a flat Universe by invoking the Cosmological constant, Λ. We should however bear in mind that Λ is still often regarded as no more than a tool which is invoked every time a problem is encountered with some model, only to be dropped again whenever a more satisfactory model is found.

In the light of the optical number counts, the recent deep infrared survey of Cowie *et al.* (1991a) has produced surprising results, as the high density implied by the optical counts is not observed in the K band. The infrared counts are thus more easily compatible with a $\Omega_0 = 1, \Lambda = 0$ Universe. The survey finds evidence for colour and luminosity evolution, with a rapid blueing of the colours beyond $K = 19$. Despite the lower density relative to the optical counts, a significant amount of luminosity *and* density evolution are still required to explain the K band number counts.

1.2.2 Cluster Galaxies and the Butcher-Oemler Effect.

The properties of cluster galaxies differ from those of field galaxies in many respects, the most fundamental difference being the Hubble type: the majority ($\approx$ 70%) of field galaxies are spirals, whereas clusters tend to contain a higher fraction of elliptical and SO galaxies (Oemler 1992). Other properties which appear to be correlated with the richness of the environment include the gas contents of spirals, the mean colour of a given morphological type and the fraction of blue galaxies relative to the total population. All of these trends would seem to indicate that the evolution of galaxies is strongly influenced by their environment, instead of it being a largely internal process occurring in all galaxies.

A photometric survey of clusters at $z \sim 0.5$ undertaken by Butcher & Oemler (1978, 1984) revealed a larger population of blue galaxies when compared to present-day clusters. This has now become known as the "Butcher-Oemler effect" (hereafter B-O effect), an equivalent phenomenon to the excess of faint blue field galaxies discussed above.

Several studies have subsequently established strong links between the B-O effect and intense bursts of star formation in some cluster members (Couch *et al.* 1992). The issue now is therefore to understand which physical processes could give rise to such enhanced starbursts. Based on an observed ring-like distribution of galaxies around the cluster centres, together with higher velocity dispersions relative to redder galaxies, Dressler & Gunn (1990) have suggested that the blue galaxies are in fact infalling field galaxies having encountered shock fronts in the intra-cluster medium. Such shocks would then trigger *ram pressure-induced star formation.* The most serious difficulty of this model is perhaps the lack of evidence that ram pressure can trigger star formation (Oemler 1992).

A recent morphological study of a $z = 0.3$ cluster (Couch *et al.* 1992) shows that the

galaxies producing the B-O effect are mainly spiral galaxies, and that mergers and interactions almost certainly play an important role in the B-O effect. This appears to corroborate the infall model, as the galaxies would then have morphological types characteristic of the present field population. Furthermore, as the merging galaxies originate outside the cluster and interact *before* entering it, the infall scenario also provides a natural explanation for the existence of mergers in a cluster environment where the high relative velocities between galaxies would tend to inhibit such events.

Allington-Smith *et al.* (1992) have carried out a survey of radio-selected groups with redshifts up to $z \simeq 0.5$. The authors list several intra-cluster processes which could provide an alternative to the ram-pressure induced model of Dressler & Gunn but conclude that their data is consistent with both the infall scenario and the internal origin hypothesis. The main conclusion drawn from their sample is that, whatever the cause to the B-O effect, it is a strongly richness-dependent process which is inefficient in low density environments.

The old populations in clusters between $z = 0.3$ and $z = 0.9$ have been studied by Aragón-Salamanca (1991), who finds clear evidence for colour evolution in that redshift range. Such evolution is believed to be due to ageing of the old stellar populations. No galaxies as red as today's ellipticals are found at $z \simeq 0.9$, implying that the bulk of the elliptical cluster population is homogeneous, sharing a common origin and epoch of star formation ($z \gtrsim 2$).

1.3 THE EPOCH OF GALAXY FORMATION

One crucial step towards understanding the evolution of galaxies is to know at what epoch they formed. The established view is that galaxies formed due to primordial fluctuations in the density field, which were then enhanced through gravitational instability. Within this framework, the most accepted theory of galaxy formation is the Cold Dark Matter model or CDM (e.g. Davis *et al.* 1985). This model, in which the bulk of the matter in the Universe is constituted by massive, weakly interacting elementary particles, implies that galaxies formed at a relatively recent epoch ($z \lesssim 2$) and only subsequently joined together to form today's clusters and superclusters, i.e. a scenario in which the large scale structure observed today originated from small scale overdensities. The strong evidence for galaxy evolution at $z \lesssim 1$ and the existence of protogalactic Ly α clouds at $z \simeq 2$ give support to this hypothesis. However, the model has difficulties in explaining the dramatic change, in so short a timescale, from the primordial mean density to the characteristic galactic density, as such a change would be expected to leave observable traces.

An important consequence of CDM theory is that it does not predict a significant number of clusters at redshifts $z \gtrsim 1$, as the relatively late epoch of galaxy formation would not leave enough time for the clusters to assemble. Although it has been firmly established that galaxy-like objects existed at $z > 3$ (e.g. Lilly 1988), the detection of a cluster at $z \simeq 1.5$ would certainly put pressure onto the CDM model. For this reason it is important to determine whether any objects detected at those redshifts are field galaxies or part of a group or cluster.

1.4 AIMS AND MOTIVATION OF THE PRESENT WORK

1.4.1 Motivation

It might appear from the above discussion that much work is still needed at low redshifts in order to understand some of the present puzzles of galaxy evolution. One might then question the wisdom of probing into even higher redshifts, where the uncertainties are far greater. However, we hope that by building an unbiased sample of high-redshift galaxies (i.e. one consisting of *normal* galaxies) we may attempt to answer some of the questions which cannot be directly addressed at $z < 1$:

1) Does the mean colour of the galaxy population at $z \simeq 1.5$ imply large amounts of evolution, or is it consistent with just passive evolution? We should bear in mind that evolutionary effects which are relatively weak at lower redshifts may be amplified due to the longer timescales involved and thus might be more easily discernible at $z \lesssim 1$.

2) What limits can we place on the epoch of star formation in galaxies by measuring the rates of star formation at high redshifts?

3) How does the normalisation of the luminosity function at high redshifts compare with the present-day value of ϕ^*, and does it explain the excess of faint blue counts in terms of mergers?

4) Can we place any constraints on the epoch of galaxy formation? Do our detections allow us to rule out any models of galaxy formation, given that the standard CDM models predict the absence of dense, bound systems at high redshifts?

1.4.2 The Strategy

Our search strategy to detect high redshift galaxies is to image the fields of QSOs showing C IV absorption lines in their spectra. The C IV doublet at $\lambda\lambda$ 1548, 1550 enters the optical region at $z \simeq 1.2$ and is detectable to redshifts $z > 4$, thus providing evidence for the presence of gas at very early epochs. It is now widely accepted that the heavy-element absorption systems in QSO spectra are indeed intervening in nature (this and other properties of the absorption systems are discussed in detail in chapter 2). While Lyman forest lines are believed to be produced by *intergalactic* material, the absorption line-galaxy connection has been firmly established for $z < 1$ Mg II systems (Bergeron 1986, Bergeron & Boissé 1991) and statistical similarities between Mg II and C IV systems (Steidel 1990, 1993a) seem to confirm that C IV absorption lines are also produced by intervening galactic halos.

Having obtained deep images of the QSO fields, we then compare the number of detected sources with that expected from random field surveys. We analyse the possible origin of any eventual excess of objects and then determine their intrinsic characteristics.

Besides the motivation outlined above, we stress the importance of our method as a reliable identifier of high redshift galaxies when compared to other available methods. The deepest spectroscopic surveys have turned out to be ineffective in locating high-redshift populations, as the bulk of the galaxies detected in such surveys have mean redshifts no higher than $z \simeq 0.5$ (Colless *et al.* 1990, Lilly *et al.* 1991). The direct detection of individual objects at high redshifts has thus so far been limited to objects with special properties such as Seyferts, radio-galaxies and quasars, which may not be characteristic of the general field population.

1.5 THESIS LAYOUT

This thesis is divided into five chapters. In chapter 1 we have given an outline of the subject of galaxy evolution, followed by a brief discussion of the epoch of galaxy formation and how the detection of galaxies or clusters at high redshifts might help place constraints on this epoch. Finally we have presented an outline of the aims and motivation behind this project and the layout of this thesis.

Chapter 2 is a review of the history of QSO absorption, from 1965 when it was first suggested that the heavy-element absorption lines observed might arise in foreground objects to the present large-scale surveys of QSO absorption lines and their statistical properties. Emphasis is given to both C IV and Mg II surveys, as several properties are shared by these two classes of absorbers.

Chapter 3 presents the data obtained in this survey, discussing the selection of the QSO sample, the observations and data reduction procedures.

In Chapter 4 the results are presented and analysed, and the implications of our findings discussed.

Finally in Chapter 5 we summarise the main conclusions drawn from our work and briefly discuss the possibility of obtaining spectroscopic confirmation of the absorbers. We conclude by proposing a strategy for extending our survey to higher redshifts.

2 THE HISTORY OF QSO ABSORBERS

2.1 EARLY WORK

The hypothesis that QSO absorption lines are produced at lower redshifts by intervening material was first raised by Bahcall and Salpeter (1965), only two years after the discovery of quasars as a new class of extragalactic objects. Subsequently, Bahcall, Greenstein & Sargent (1968) detected four absorption systems with $z_{abs} \ll z_{em}$ in the spectrum of PKS 0237−23, a QSO at $z = 2.22$, and discussed the two most likely hypotheses for the origin of the systems, namely that they arise either in gas clouds surrounding the QSO or in foreground galaxies. The authors stressed, however, that a definitive decision in favour of either of these hypotheses was at the time impossible, and that the only conclusive evidence in favour of the intervening hypothesis would be the detection of an optical or radio galaxy at the absorber redshift.

In subsequent years, the procedure commonly adopted to verify the above hypotheses was to identify those QSOs which have absorption lines at lower redshifts and *then* search for the objects producing the absorption. But, initially, the reverse was attempted: the QSO 3C232 was known to lie behind a nearby spiral galaxy, NGC 3067. Haschick &

Burke (1975) searched for absorption lines in the QSO's spectrum and found that the redshifts of the 21 cm and the Ca II H and K lines were identical to that of the foreground galaxy, thus confirming that not all the absorption lines seen in a QSO spectrum were necessarily physically related to the QSO. Although a valid test of the extrinsic origin of certain absorption systems, this method was severely limited by the fact that all known galaxies were at redshifts less than $z \simeq 0.2$. This restricted ground-based observations to searches for Ca II H and K and HI at 21 cm, which are considerably more difficult to detect than, e.g., the Mg II doublet at $\lambda\lambda$ 2795,2802.

The first direct attempt at detecting QSO absorbers was made in 1978 by Weymann *et al.*, who imaged the fields of six QSOs known to have Mg II absorption systems at redshifts $z_{abs} \leq 0.6$. They found several objects with a mean projected distance of $\simeq$85 kpc if assumed to be at the absorbers' redshifts. However, spectroscopy of the candidate sources did not confirm any of the expected redshifts and thus no positive identifications of absorbers were made.

2.2 LARGE SCALE SPECTRAL SURVEYS AND THE PROPERTIES OF HEAVY-ELEMENT ABSORBERS

In this section we discuss the properties of heavy-element absorption systems, paying particular attention to C IV systems. The Mg II absorption line surveys are briefly reviewed and their results compared with those of C IV surveys.

Studies of the properties of C IV absorbing systems were initiated in the early 1980s with the start of extensive high-resolution surveys of QSO spectra (e.g. Young, Sargent and Boksenberg 1982, Foltz *et al.* 1986, Tytler *et al.* 1987). One of the most important C IV

surveys is that of Sargent, Boksenberg & Steidel (1988, hereafter SBS), a discussion of which is presented here.

SBS observed a total of 52 QSOs in the reshift range $1.8 \leq z_{em} \leq 3.6$, with a resolution of 0.8 or 1.5Å. Their only criteria for selecting the QSOs were that they have a redshift $z_{em} \geq 1.8$ and visual magnitude $V \leq 18.0$. Thus their sample can be considered as unbiased for absorption line studies as it was constructed without any *a priori* knowledge of the QSOs' spectral features.

In their complete sample SBS measured a total of 229 C IV $\lambda\lambda$ 1540,1550 doublet redshifts, from which several statistical properties of the absorbers were inferred. Globally, these properties are interpreted as reflecting the initial heavy-element enrichment in interstellar gas and the evolution in the ionization state of the halo gas with time. The main conclusions were:

1. The large-scale distribution of absorber redshifts per QSO sightline is Poissonian, and therefore consistent with the intervening hypothesis.

2. There is cosmological evolution in the number density of absorbers per unit redshift, which decreases with increasing lookback time.

3. There is a systematic change in the C IV doublet ratio with redshift which, together with (2) above, is interpreted as a systematic change in the abundance of carbon in the absorbing clouds.

4. Significant clustering of C IV systems is detected on scales of up to 600 kms^{-1}. This is more likely to be due to galaxy-galaxy clustering than to relative motions of gas clouds in the absorbing galaxy.

5. There is no tendency for the absorption redshifts to cluster around the emitter, regardless of the radio or X-ray properties of the QSO.

6. No correlation is found between a QSO's luminosity and the number of absorbers along its line of sight, which implies that gravitational lensing cannot play an important role in the observed density of absorbers.

2.2.1 The Redshift Distribution of C IV Absorbers

The number of absorption systems per QSO sightline and their redshift distribution provide the most important tests as to the origin of the absorbers. Indeed if absorption is caused mainly by intervening objects (ie if the absorbers lie at the cosmological distances implied by their redshifts), then their number per QSO sightline should obey a Poissonian distribution and they should have a flat distribution in velocity. Given a sufficiently large sample, statistical tests can be carried out to verify the distributions and thus confirm or discard the hypothesis.

a) Velocity Distribution:

The difference between an absorption redshift z_{abs} and the QSO's redshift z_{em} can be expressed as a fraction of the velocity of light, using the expression

$$\beta = \frac{v}{c} = \frac{(1+z_{em})^2 - (1+z_{abs})^2}{(1+z_{em})^2 + (1+z_{abs})^2}. \qquad (2.1)$$

The β distribution turns out to be remarkably flat in the C IV samples of both SBS and Young, Sargent and Boksenberg (1982, hereafter YSB), with no strong tendencies towards clustering around β=0. Several absorption redshifts in the SBS sample are found

to have large negative relative velocities with amplitudes up to 3700 kms^{-1}, thus too large to be explained by peculiar motions in clusters. Whilst it is most likely that such large negative velocities arise in clouds surrounding the QSO, the authors point out that a substantial amount of absorption near the emission redshift imposes uncertainties in the determination of z_{em} which may be as large as a few thousand kms^{-1}.

b) Number of systems per sightline: the Bahcall-Peebles Test.

Bahcall and Peebles (1969) proposed a statistical test to investigate the deviation of the number of absorbers per QSO sightline from a Poissonian distribution. Details of the test and its application to the C IV samples are given in YSB. The number distribution obtained in YSB and in the larger sample of SBS showed no significant departure from those expected for a Poissonian distribution, and the data were therefore deemed to be consistent with (and thus confirm) the hypothesis that absorption redshifts are produced by cosmologically distributed intervening objects. Since the 1982 paper of YSB it has generally been accepted that heavy-element absorption systems are indeed produced by intervening objects.

2.2.2 Properties of C IV Systems: Evolution with Redshift.

Three different types of evolution with redshift can be studied in a sample of C IV systems: the evolution in number density, the evolution of line strength and the evolution of doublet ratio. Each in turn provides complementary information on the state of the absorbing gas at different epochs.

a) Number density Evolution:

For Friedmann cosmologies with $\Lambda = 0$ and deceleration parameter q_o, the number density $N(z)$ as a function of redshift of cosmologically distributed intervening absorbers is expected to follow the expression

$$N(z) = N_o(1+z)(1+2q_oz)^{-1/2}, \tag{2.2}$$

provided the absorber properties do not evolve with redshift. N_o, the local value of $N(z)$, is given by

$$N_o = \sigma_o\Phi_o c/H_o, \tag{2.3}$$

with σ_o being the absorber cross-section (assumed to be constant) and Φ_o the constant comoving number density. If the absorbers do evolve with redshift, then N_o=$N(z)$. The original derivation of the above expression is due to Wagoner (1967).

To apply this study to an observed data set, it is convenient to express equation (2.2) as a power law of the form

$$N(z) = A(1+z)^\gamma, \tag{2.4}$$

where A is a constant. We can then obtain, via a maximum likelihood estimate, a value for γ which will indicate the amount of evolution present in the sample.

SBS found a *decreasing* trend in $N(z)$ as z increases. Although the slope varied according to the sample selected, the trend was verified in all samples, irrespective of the minimum

equivalent width or other considerations which constrained the samples, such as minimum velocity dispersion (βc). As an illustration, for their complete sample (229 systems), the authors find $\gamma = -0.9 \pm 0.4$ and, for their sample "S2", $\gamma = -1.2 \pm 0.7$. S2 may be considered as a statistically more appropriate sample as it considers as a single system all those with $\beta c \leq 1000$ kms^{-1}, and thus avoids counting a multiple system more than once.

How is this observed negative evolution interpreted? For the different samples of SBS, it was noticed that the curve tended to flatten out as the minimum equivalent width which defined a sample decreased, to a point where a sample with a very small $W_{r,min}$ was even consistent with no evolution. This might suggest that the evolution witnessed is in the *strength* of the absorbers rather than their numbers, with the mean strength of the C IV doublet decreasing with increasing redshift.

In an attempt to resolve these questions, Steidel (1990) extended the work of SBS by adding 11 high-redshifts QSOs to the sample of 55, totalling 275 absorption redshifts and considerably extending the redshift range of the sample. Using this enlarged sample, the maximum likelihood fit gave a value of $\gamma = -1.26 \pm 0.56$, in close agreement with that of SBS (sample S2) but with a slightly smaller error. The sample was then arbitrarily divided into two subsets, one with $0.15 \leq W_o(1548) < 0.40$Å and the other with $W_o(1548) > 0.40$Å, and this division revealed a marked dependence of the observed evolution on equivalent width: the "strong" sample shows a decreasing trend, with $\gamma = -2.35 \pm 0.77$ whereas the "weak" sample has $\gamma = 0.14 \pm 0.85$, thus broadly consistent with no evolution in density. It is clear therefore that what we are witnessing here is a significant evolution in the *strength* of the C IV doublet with redshift. The possible causes for this observed evolution in C IV strength are discussed in section 2.2.3.

b) Line-strength Distribution and Evolution with Redshift.

Provided the doublet is not saturated (this is observed to be the case only at redshifts $z \geq 2$; Steidel 1990, 1993a), the equivalent width of the λ1548 line provides a direct measure of C IV column density in the absorbing system and thus by studying its evolution with redshift we can obtain information about the evolution of the absorbing gas density with time.

The fit of an exponential function to the distribution of equivalent widths (usually applied to to the distribution of Lyman forest line strengths) was not well suited to the samples of both SBS and Steidel (1990), who found a large excess of low equivalent width ($W_o(1548) \leq 0.2$Å) C IV doublets. This excess is comparable to that found for Lyman forest lines by other observers (e.g. Carswell *et al.* 1984, Atwood, Baldwin and Carswell 1985, Murdoch *et al.* 1986). A broad peak from $W_o = 0.5$Å to $W_o = 0.7$Å is seen in the sample of Steidel, and analysis of the C IV curve of growth shows that this region corresponds to C IV column densities of log N(C IV)= 13.8 – 14.3.

The evolution of equivalent width with redshift is a difficult parameter to establish due to the small number of redshifts available compared to, e.g., Lyman forest systems. For a sample of 90 systems, no correlation between $W_o(\lambda1548)$ and redshift was found by SBS. Steidel (1990), however, finds a significant difference in the equivalent width if the sample is split into high (≥ 2.2) and low (< 2.2) redshift, implying a considerable increase in the density of C IV with decreasing redshift.

c) Evolution of Doublet Ratio with Redshift

The ratio of the C IV doublet, defined as $DR = W_o(1548)/W_o(1550)$, also provides a quantitative measure of the C IV column density. DR can take values between 1 and 2, such that N(C IV) is higher for smaller values of DR. SBS find that DR becomes systematically larger at higher redshifts, thus in agreement with the result outlined in (*b*) above. The correlation was examined in more detail by Steidel (1990), who quantified the evolution in DR from 1.35 at $z_{abs} \sim 1.5$ to 1.65 at $z_{abs} \sim 3.0$. Such a change corresponds to an increase by a factor of ~ 3 in the mean C IV column density as we evolve from $z_{abs} \simeq 3$ to $z_{abs} \simeq 1.5$.

2.2.3 General Conclusions About the Evolution of C IV Systems.

From all of the above considerations, a picture emerges which suggests an extreme change in the distribution of C IV equivalent widths with redshift, with weak systems becoming systematically stronger with time. We now ask what factors are most likely to cause this observed change in column density: is it due to a change in the chemical abundance of carbon in the gas cloud, or rather to a change in its ionization level?

Several arguments arise against a possible change in the ionization level of the gas clouds. As C IV weakens, an *increase* in the strength of singly ionized species like C II and Si II would be expected but is not observed (Steidel 1993a); on the contrary, their strength tends to decrease with increasing redshift, in a trend rather like that of C IV (York *et al.* 1992; Steidel and Sargent 1992). A second argument is related to the origin of the ionizing radiation: as the gas clouds seem to extend for at least a few tens of kpc, it is most likely that the main source of ionizing radiation will be in the form of field radiation

from QSOs and star-forming galaxies. Thus any substantial change in the ionization level of the clouds with redshift should be due to a corresponding change in intensity of the field radiation. Recent work by Bajtlik, Duncan and Ostriker (1988), however, rules out significant changes in the radiation field intensity over the range $1.5 \leq z \leq 3.5$.

The third argument is brought forward by the similarities between C IV systems and Lyman Limit Systems (LLS). Despite some controversies about a possible identical origin of the LLSs and the C IV systems, their common properties seem to imply that, at least at high redshifts, both systems are drawn from the same population of absorbers, with the LLSs tracing the HI component of the absorbing clouds (Steidel 1990). This should therefore enable a direct comparison of the $N(z)$ behaviour of both systems, and any observed change in ionization state should be seen in both systems. However, a change in the ionisation state of the LLSs would imply an increase by a factor of 3 in the number density of LLSs between $z = 1.5$ and $z = 3.0$, incompatible with observations which show no $N(z)$ evolution in the range $0.2 \leq z_{abs} \leq 4$ (Sargent, Steidel and Boksenberg 1988; Lanzetta 1988). If we can indeed draw parallels between the properties of C IV and LLSs, then this severely constrains any evolution in the ionization state of the gas responsible for C IV absorption.

Having examined the possibility of a change in the ionization level of the absorbing clouds, we are left therefore with the most probable hypothesis that the observed evolution of the C IV systems reflects a change in the mean abundance of that element with redshift.

2.2.4 Statistical Properties of Mg II Systems.

We now briefly examine the statistical properties of Mg II systems, comparing them with those of C IV systems described above. Given that the Mg II doublet can only be observed

optically up to $z \simeq 2.2$, it is clear that any observed differences in abundances, number density, etc. between Mg II and C IV absorbers might be due to the different redshift ranges sampled.

The large scale distribution of Mg II absorbers shows the same properties as those of C IV in that there is no tendency for z_{abs} to cluster around z_{em} and the absorbers are uniformly distributed in velocity space.

No evolution in number density is observed in the analysis of Steidel & Sargent (1992), who find, for a sample of 111 systems with $W_o(\lambda 2796) \geq 0.3\AA$, $\gamma = 0.78 \pm 0.42$ (see section 2.2.2), a value consistent with no evolution for $0.0 \leq q_o \leq 0.5$. This value is also in close agreement with that obtained for Lyman Limit systems (Sargent, Steidel and Boksenberg 1989), giving rise to the claim that Mg II and Lyman Limit systems arise in the same absorber populations (recall that a similar claim was made about the common origin of C IV and Lyman Limit systems).

The strong dependence of γ on W_o^{min} when the different samples of Steidel & Sargent (1992) are compared suggests a systematic change in the Mg II rest equivalent width with redshift: the Mg II lines become progressively stronger with increasing lookback time. This trend is contrary to the behaviour of C IV equivalent widths (§2.2.2) and cannot be explained by changes in the ionization level or abundance of Mg II . It is suggested that this change is the result of evolution of the kinematic properties of the absorbing gas, either through a change in the velocity spread of the components or in the number of components, i.e. in the number of gas clouds in a given galaxy as a function of time.

2.3 IMAGING SURVEYS OF Mg II ABSORBERS

2.3.1 The Survey of Bergeron and Boissé

Bergeron and Boissé (1991, hereafter B&B) imaged a set of ten QSOs, all known to have Mg II absorption systems at low redshifts ($< z_{abs} > \simeq 0.5$). Combining those with previously published data, they formed a sample of 17 candidate absorbers, of which 13 were positively identified via imaging and subsequent spectroscopy. In all but one case, the confirmed absorber was the closest object in the sky to the QSO, always at angular separations $\theta < 15.''0$. The goals of their search, besides statistically confirming the intervening hypothesis, were to infer properties of the absorbing halos such as luminosity, size and stellar content, and to compare them with the properties of galaxies at similar redshifts found in deep surveys.

The QSOs were selected from early spectral surveys, the only selection criterion being that the Mg II lines have a velocity parameter $\beta > c/3$, to avoid selecting QSOs with $z_{abs} \approx z_{em}$. All the QSOs had an emission redshift range $0.4 < z_{em} < 2.7$, and the Mg II systems were in the range $0.16 < z_{abs} < 0.85$.

a) Magnitudes and Luminosities.

The mean magnitude of the Mg II absorbers is $R = 21.0$, with the individual values spreading over the range $19 \leq R \leq 23$. This spread is not due to any intrinsic properties of the absorbers but simply to their different redshifts, the mean of which is $\overline{z} = 0.45$. This is confirmed by their absolute magnitude distribution, which exhibits a sharp peak at $M_R = -21.4$ for $H_0 = 50$ kms^{-1}kpc^{-1} (c.f. $M_R^* \simeq -21.1$, B&B). A steep fall-off observed towards the faint end cannot be ascribed to incompleteness, since it occurs two

magnitudes below the limiting magnitude of the sample, $R_{lim} \sim 23.0$. All absorbers in the sample are therefore intrinsically bright, with none having $L < 0.3L^*$. This distribution will be compared to our own candidate absorber magnitudes when we come to discuss the hypothesis that our candidate C IV absorbers are in fact lower redshift Mg II absorbers.

B&B examined the combined effect of evolution and k-correction when calculating absolute magnitudes. They assigned assigned a Hubble type to each absorber by measuring its [OII] equivalent width, and then made use of the synthetic spectral models of Rocca-Volmerange and Guiderdoni (1986) to estimate the overall effect of $e(z) + k(z)$. They found that the relevant range of corrections ranged from 0 to -0.3 and that, in view of the uncertainties involved in determining their values, no correction was appropriate.

b) Halo Sizes and Impact Parameters.

Understanding halo evolution is important in that it provides detailed information on the physical conditions prevailing at early epochs of galaxy history, particularly kinematics and chemical abundances. The work of B&B should allow us to compare the properties of their Mg II absorbing halos with those of our candidate absorbers and thus place constraints on the evolution of halo sizes and numbers on a relatively large time baseline.

If we consider the optical size of a typical galaxy ($R \simeq 10$ kpc) and the present-day galaxy luminosity function, it turns out that the number of galaxies likely to lie along the line of sight to a given QSO is much smaller than the observed number of absorption systems, and thus the optical regions of galaxies alone cannot account for the observed absorber density (Wagoner 1967). To explain this discrepancy, Bahcall and Spitzer (1969) first suggested that galaxies had very extended halos in the past, which became

gradually smaller as star formation was triggered by cloud collisions. By making a few assumptions about the absorber properties we can ask how large would galaxy halos have to be in order to explain the observed absorber density.

To estimate the size of the absorbing halos, let us assume a Schechter (1976) luminosity function for the absorbing galaxies, a Radius-Luminosity relation of the form $R \propto L^{\beta}$ (Holmberg 1976, with $\beta = 0.4$) and a low luminosity cut-off L_{min}. The Schechter luminosity function is given by

$$dn = \Phi^* x^{-5/4} e^x dx, \tag{2.5}$$

where $x = L/L^*$, $\phi^* = 3 \times 10^{-3}$ Mpc^{-3} and $M_B^* = -20.6$ (de Lapparent *et al.* 1989). It is assumed that the local luminosity function remains valid at $z = 0.4$. With the further assumption that all galaxies brighter than L_{min} are surrounded by spherical halos, the halo radius of an L^* galaxy is then given by

$$R^*(z) = (\sigma^2(z)/\pi)^{0.5} = 6.62 R_H \left(\frac{dN/dZ}{1+z}\right)^{0.5} \Gamma(a, x_{min})^{-0.5}, \tag{2.6}$$

where $\Gamma(a, x_{min})$ is the incomplete gamma function ($a = \alpha + 2\beta + 1$), $x_{min} = L_{min}/L_*$ and R_H is the Holmberg radius of a galaxy, defined as the radius at which the B isophote is 26.5 mags arcsec^{-2} (Holmberg 1976). The radii measured or predicted by B&B are given in terms of R_H so as to eliminate the dependence on H_o, and the value used is $R_H = 22$ kpc for an L^* galaxy at $z = 0$.

For the Bergeron and Boissé sample, x_{min} is estimated via a direct comparison with the R magnitudes of the absorbers (recall $< M_R >= -21.4$). This comparison is made possible by the fact that the R band coincides (to better than 3%) with the rest-frame B-band at the mean redshift of the absorbers. The values obtained are then $x_{min} = 0.5$

and $< L/L_* >=< x >= 1.3$. Applying this procedure to the $W_o(\mathrm{Mg\,II}\ \lambda 2796) \geq 0.6$Å sample of Sargent, Steidel and Boksenberg (1988), B&B find a predicted mean halo radius

$$R^* = 4.2 R_H. \tag{2.7}$$

Thus they predict that the average absorber will have a cross-sectional radius of $\sim 90 h_{50}^{-1}$ kpc. It should be noted however that the above estimate of R^* is dependent on several assumptions and is therefore subject to considerable variations. For example, the value of $\beta = 0.4$ for the index in the $R \propto L^\beta$ scaling law has recently been reinforced by Bechtold and Ellingson (1992) but challenged by Steidel (1990), who finds $\beta = 0.2$ (see section 2.3.2).

The confirmed absorbers are found to have impact parameters $0.5 \leq D/R_H \leq 4$, with a sharp peak around the mean value, $< D/R_H >= 2.34$ or $D \sim 50 h_{50}^{-1}$ kpc ($q_o = 0$). The data are compatible with $0 \leq \beta \leq 0.4$, and thus there is no significant disagreement with the predicted halo radii, bearing in mind that impact parameters only provide a lower limit to R^*, since the radius of an absorber can be of any size larger than its impact parameter.

The shapes of the absorbing halos are also compared with those predicted from geometrical considerations, and it is found that the observed distribution of impact parameters matches closely the predicted distribution of spherical halos. A highly elongated geometry is rejected at the 99% confidence level, as it would require much larger impact parameters than those measured. Such absorbers would have much smaller cross-sections and hence could not account for the observed number of Mg II systems per line of sight.

c) Equivalent width of the [OII] λ 3727 line: Star Formation and Morphology.

One considerable advantage of Mg II absorbers over C IV absorbers is that in the former case it is easier to obtain spectra of the candidate absorbers and thus unambiguously confirm or discard them as responsible for the observed absorption systems. This is due not only to the fact that the smaller absorber redshifts translate into brighter apparent magnitudes for a galaxy of a given luminosity, but also to the fact that the [OII]λ 3727 line is accessible as a reliable redshift identifier.

The [OII] emission line offers several advantages when used as an indicator of star formation in a system: being a remarkably strong feature, it is easily measurable even at the Mg II absorber redshifts; it is observable in the optical window for the entire redshift range of the sample; and, most importantly, its equivalent width is an *instantaneous* indicator of star formation, unlike e.g. Balmer absorption lines or the 4000Å break, which only provide a measure of star formation over a period of at least a few Gyr (Broadhurst *et al.* 1988). On the other hand, the [OII] line alone does not provide a quantitative measure of the star formation rate, for which a measure of the excitation level of the gas is needed.

The [OII] flux was measured in all the absorbers of B&B, and most showed strong emission, with only 23% having $W_o < 10$Å. Thus most Mg II absorbers show signs of strong star-forming activity.

Any comparison of the [OII] properties of the absorbing galaxies must be made with field galaxies at similar redhifts, so as not to measure purely evolutionary effects. B&B therefore compared the [OII] rest equivalent width distribution of their sample with that of the Durham Faint Galaxy Surveys (Broadhurst *et al.* 1988; Colless *et al.* 1990), finding no statistically significant differences in the distribution. Aside from the redshift

distribution, selection effects also have to be considered when comparing two different samples. One could claim that, since the Durham Survey galaxies were selected from b_j images and the absorbers from R images, the latter would tend to be redder and therefore show less significant star formation than the field sample. The authors argue however that this does not produce a significant bias, since the detection limit of their survey is considerably fainter than their absorber magnitudes, implying that much bluer objects could still have been detected.

Having taken into consideration the effects described above, it is concluded that the similarity in the W_r[OII] distribution reflects similar star formation histories in the Mg II absorbers and the field galaxies of the Durham surveys.

Although nearly all absorbing galaxies are unresolved, spiral types are generally favoured over ellipticals, due to both the presence of [OII] emission and the moderately high absolute luminosities of the absorbing galaxies. The morphology has been confirmed in at least one case in which the absorber shows a bulge and edge-on arms. Furthermore, in the hypothesis that mergers play an important role at $z \sim 0.4$ (e.g. Broadhurst *et al.* 1992), then a certain number of irregular galaxies are also expected to be present in the sample.

d) The Absorbing Galaxies' Environment

We might now ask whether the confirmed absorbers belong to groups or clusters or are just field galaxies. For this question to be properly addressed, it would have been necessary to compare the number of objects detected with field counts. This was, however, beyond the scope of B&B's work. On the basis that no two similar redshifts are detected in any of the QSO fields, they simply argue that the absorbers detected are field galaxies

or that they belong at most to loose groups (Bergeron 1988).

2.3.2 The Survey of Steidel

A larger imaging survey of Mg II absorbers, similar in aim and method to that of Bergeron & Boissé, is being carried out by Steidel (1993a, 1993b). The sample consists of 55 galaxies, imaged in both optical and near-infrared bands and followed-up spectroscopically. The much larger number of galaxies should place tighter constraints on all of the absorber properties studied by B&B. Some preliminary results are outlined below.

The luminosity function of the absorbers has been compared to the recent b-band luminosity function of Loveday *et al.* (1992). Both are found to be remarkably similar in shape and normalisation if one allows for a small amount of luminosity evolution ($0^m.5$ brighter at $z \simeq 0.6$). Virtually all absorbers are within two magnitudes of a present-day L^* galaxy. Furthermore, the luminosity function has a faint cut-off at $L \sim 0.2L^*$, implying that dwarf galaxies cannot make a significant contribution to the total gas cross-section.

The colours are also compared with those of present-day field galaxies. The sample shows the colours of typical mid- to late-type spirals, with the reddest galaxy in the sample having the colour of an Sab spiral, $(R-K) = 3.8$. None of the galaxies have very blue colours indicative of substantial star formation, implying that the relatively bright B luminosities observed are not just the result of starbursts. A further factor which confirms the above is that the [OII]λ3727 line is either weak or absent in several of the galaxies, in contrast with the sample of B&B, where most absorbers show strong [OII] emission.

The geometry of the gaseous halos is inferred from the absolute magnitude and im-

pact parameter distributions. In accordance with the result of Bergeron & Boissé, the distribution strongly favours spherical halos rather than flat/linear ones, a result also confirmed by the recent work of Bechtold & Ellingson (1992). However, Steidel finds a value for β of 0.2, implying a much weaker dependence of halo radius on the galaxy's luminosity and hence implying a smaller halo size for L^* galaxies. The absorbers have a mean impact parameter of $R \simeq 35$ kpc (c.f. $R \simeq 50$ kpc in the B&B sample).

2.3.3 A Search For Mg II Absorption Produced by Known Galaxies

Recently, Bechtold & Ellingson (1992) have adopted a reverse approach by undertaking a spectroscopic survey of QSOs lying at small angular separations from known galaxies, thus searching for Mg II absorption lines at the redshifts of previously identified galaxies. Their aim is to increase the sample of absorbers at known redshifts in order to investigate several properties, such as a possible correlation of Mg II equivalent width with impact parameter which would provide clues to the gas column density distribution in the absorbing halos. Another issue to be addressed is determining whether the absorbing clouds arise within the galaxies' halos or rather in dwarf satellite galaxies, by investigating the distribution of cloud velocities relative to the bulk of the galaxy's light. Initial results point to an absorption line detection rate of only $\sim 25\%$ which when compared to Bergeron & Boissé's 80% success rate implies a halo covering factor of only ~ 0.25.

Comparisons between absorbing and non-absorbing samples showed no significant differences between their absolute magnitude distributions, thus reinforcing the claim by Steidel (1993a) that Mg II absorbers provide a fair sample of "normal" galaxies at earlier epochs and therefore represent a very important population for studying galaxy evolution from those epochs to the present day.

Naturally the possibility remains that Mg II absorption is caused by objects other than large gaseous halos around bright galaxies, e.g. it could arise in low surface brightness galaxies (Phillipps *et al.* 1992). Observational projects are now under way to test this hypothesis further.

2.4 COMPARISON OF Mg II AND C IV STUDIES

Before embarking on Chapters 3 and 4, which will deal with our own C IV survey, we briefly review the principal differences between the Mg II surveys that have been discussed in this chapter and our own work on C IV systems.

The aim of the pioneering survey of Bergeron & Boissé was mainly to establish *what kind of objects* give rise to the heavy-element absorption lines in QSO spectra. Thus it was natural to try and detect those systems producing Mg II absorption rather than C IV , given that the lower redshifts would imply brighter apparent magnitudes, and thus enable a somewhat easier identification and subsequent spectroscopy of candidate sources. Building a sizeable sample of intermediate redshift galaxies in order to infer their evolutionary properties was a secondary concern that could only be addressed after confirmation of the candidates' redshifts. This is now being undertaken by Steidel (1993a, 1993b).

In the case of C IV systems, the substantial difficulties involved in obtaining spectra at redshifts $z \geq 1$ mean that there has been to this date no direct confirmation of the nature of the absorbers. However, given the remarkable detection rate of Bergeron & Boissé and the observed similarities between C IV and Mg II systems, we consider it now

reasonable to *assume* that C IV absorption is also produced by galactic halos which, notwhitstanding their different evolutionary stages, are essentially the same objects as the Mg II absorbers. Thus we bypass the initial stage of confirming the origin of the absorption lines before analysing the properties of the absorbing galaxies. Naturally in this process we are forced to adopt a more statistical approach and infer properties of the whole sample before attempting to obtain individual redshift confirmation. Hence, contrary to previous work on Mg II , a mean redshift for the absorbers is assumed before we calculate distance-dependent properties such as absolute magnitude and linear impact parameter. We also resort to statistical arguments to discard the possibilities that the absorbers lie at lower redshifts or are physically associated with the QSO.

Despite the technical limitations, it is still a goal of this project to obtain spectra of the most promising candidates. In the absence of strong emission lines such as [OII]λ3727 (which is redshifted out of the optical window at $z \simeq 1.3$), we will have to resort to weaker rest-frame UV lines which require higher signal-to-noise.

We should note however that, despite the considerable difficulties, the rewards are substantially higher when studying C IV absorbers since we are greatly extending the time baseline for galaxy evolution. On a longer term, we can hope to answer questions that could not be addressed by studying Mg II galaxies at redshifts $z \simeq 0.5$. Comparing galaxy properties at our mean absorber redshifts, $z \simeq 1.6$, with their present-day counterparts allows us to compare today's galaxies with what may have been their precursors at an epoch close to that of galaxy formation.

3 OBSERVATIONS & DATA REDUCTION

3.1 SELECTION OF THE QSO SAMPLE

The QSOs we have imaged were selected from several of the extensive spectral surveys discussed in Chapter 2. Individual references are given in table 3.1. Our choice was based primarily on the number of clustered C IV absorption systems present in the spectra. Ideally we would select two samples, one containing C IV absorption lines and another *without any absorption lines* which would act as a control sample for field count determination. Such an approach is unfortunately unrealistic from the point of view of telescope time: the time needed for imaging a single field to $K \simeq 20.4$, including overheads, is over six hours. In order to maximise our chances of detection, therefore, we chose to observe QSOs showing clustered absorption lines in their spectra and use published field counts for field subtraction (the procedure is described in detail in chapter 4). The criterion used in the selection was that each QSO should have at least two clustered C IV doublets within a rest-frame dispersion $\Delta z \simeq \pm 0.01$, which at $z \simeq 1.5$ corresponds to $\Delta v \leq 1000$ kms^{-1}, a typical value for intra-cluster velocities.

One fundamental point when constructing an unbiased sample of galaxies at redshifts $z > 1$ would be to ensure, whenever possible, that the objects eventually detected are not

lower redshift galaxies as found in earlier Mg II surveys and that they are not associated with the QSO itself, as the QSO environment might alter the properties of the galaxies in such a way that we could no longer consider them "normal". Thus when selecting an unbiased sample we would *ideally* exclude:

(i) QSOs which show absorption systems at $z_{abs} \approx z_{em}$.
(ii) Radio-loud QSOs, since these have a higher tendency to have associated clustered galaxies than radio-quiet ones (see e.g. Yee & Green 1987).
(iii) QSOs with strong Mg II absorption systems.

In practice however our sample selection was restricted by the optical data available; furthermore, the abundance of Mg II systems in QSO spectra is such that eliminating all QSO with $z < 1$ Mg II systems would drastically reduce the number of candidate fields. Although all of our selected QSOs meet criterion (i) above, our current sample contains 9 radio-loud QSOs (Hewitt and Burbidge 1987) and four also have lower redshift Mg II systems.

The possibilities that our absorbers are physically associated with the QSO or with Mg II systems at lower redshifts are discussed in detail in Chapter 4.

3.2 THE IMPORTANCE OF OBSERVING DISTANT GALAXIES IN THE INFRARED

Important differences exist in the spectral energy distribution of galaxies across the Hubble sequence. The most striking differences appear in the rest-frame UV and blue optical regions and reflect the amount of star formation occurring in a system. On the

Table 3.1. QSO Coordinates and Emission Redshifts.

QSO	α (1950.0)	δ (1950.0)	z_{em}	Reference
Q0013−004	00 13 28.7	−00 29 05	2.086	1
Q0151+048	01 51 17.4	04 48 15	1.904	1
BLL0215+015	02 15 14.2	01 30 59	1.715[a]	2
Q0237−233	02 37 52.7	−23 22 09	2.222	1
Q0421+019	04 21 33.0	01 57 33	2.051	3
Q0424−130	04 24 48.0	−13 09 36	2.166	1
Q0836+195	08 36 15.0	19 32 24	1.691	4
Q0854+191	08 54 36.5	19 07 00	1.896	1,4
Q1329+412	13 29 29.9	41 17 23	1.930	1
Q1331+170	13 31 10.1	17 04 26	2.081	1
Q2044−168	20 44 30.8	−16 50 09	1.939	4

(a) uncertain.

References: (1) Sargent, Boksenberg & Steidel (1988); (2) Blades *et al.* (1982); (3) Young *et al.* (1982); (4) Foltz *et al.* (1986).

other hand, the far-red and near-infrared continua of a galaxy represent the underlying populations, as they are largely dominated by the light of older stars unrelated to recent star formation. Typically, in a 10^7 year-old single-burst galaxy, the total flux contribution from main-sequence stars is over 70% in the B band, decreasing to 30-40% in R and less than 10% in K (Bruzual & Charlot 1992).

At $z > 1$, the UV rest frame of a galaxy is shifted into the optical window, while the optical rest-frame moves into the infrared. Thus by studying high-redshift galaxies in optical passbands we would be looking primarily at the light from hot, young stars and we would therefore be favouring the detection of the bluest, most star-forming systems. Selecting galaxies in the infrared therefore avoids this unwanted bias.

Furthermore, the best studied parts of nearby galaxies' spectral energy distributions are the optical regions, and we must be able to compare present-day and high-redshift galaxies *in the same spectral range* if we are to draw any conclusions about their evolution. Also, the uncertainty involved in determining the k-correction is reduced in the infrared, as its value is considerably smaller (in fact negative, see chapter 4) and less type-dependent than in visual passbands.

The importance of selecting high-redshift galaxies in the infrared is illustrated in figure 3.1, which shows a comparison of the exposure times needed to detected non-evolved L^* galaxies of various Hubble classes in the R, I and K bands. Note that the lines are parallel for all types of galaxies in the K band. The same is not true in R, where the detection of a normal E-type galaxy at $z \approx 1.5$ requires a considerably longer exposure than for a spiral galaxy at the same redshift. Thus the K band ensures the selection of a fair sample, as the fraction of each type of galaxy detected is largely identical at any redshift.

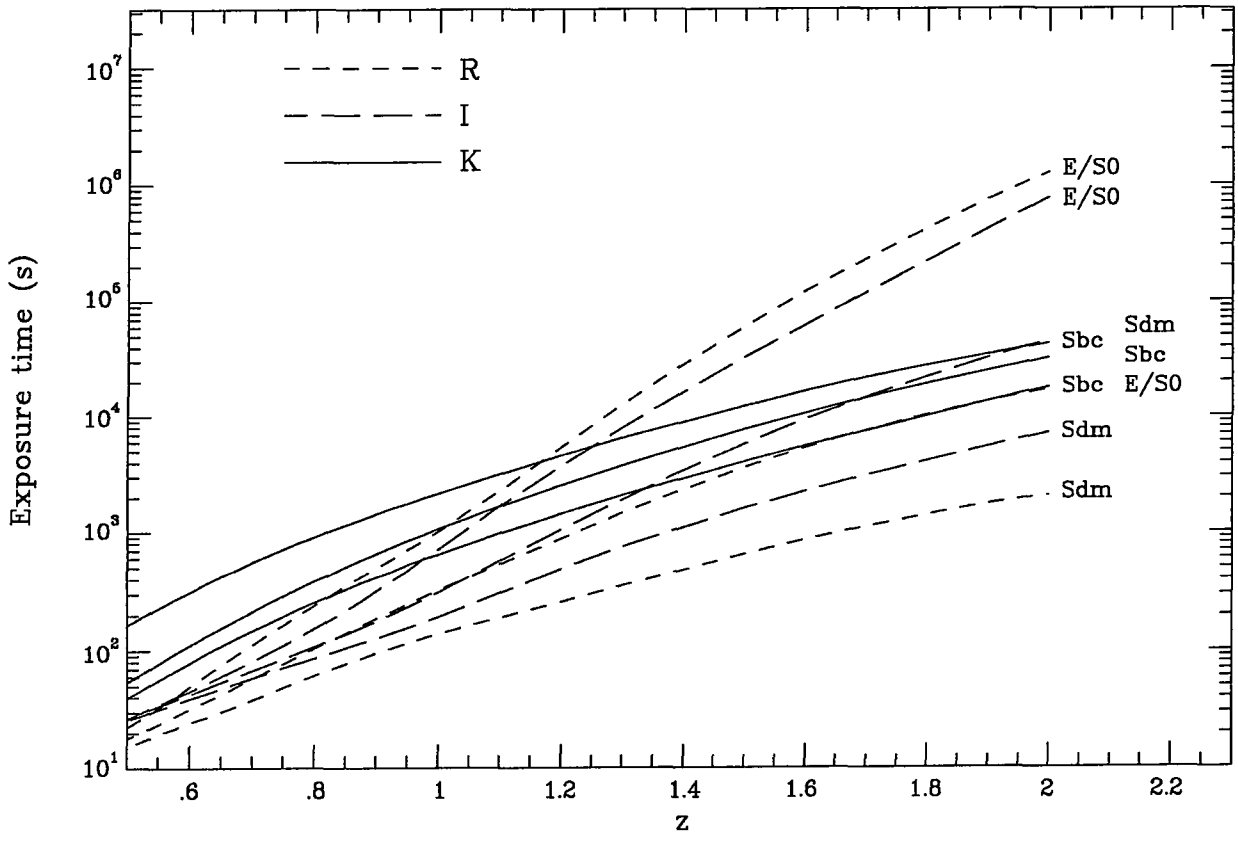

Figure 3.1 Exposure times needed to detect non-evolved L^* galaxies of different Hubble classes in the R, I and K passbands (Aragón-Salamanca 1991).

3.3 THE INFRARED OBSERVATIONS

3.3.1 IRCAM

All the infrared data used in this project were obtained during two observing runs on 14-18 October 1991 by A. Aragón-Salamanca and 7-10 March 1992 by R. S. Ellis and the author.

Images were obtained using the IRCAM camera (McLean 1986) at the f/36 Cassegrain focus of the 3.8 m UK Infrared Telescope (UKIRT), situated on the summit of Mauna Kea, Hawaii, at an altitude of 4200 m. The site benefits from excellent conditions, with frequent sub-arcsecond seeing. Mauna Kea offers another important advantage in that, being above 60% of the Earth's atmosphere, it has very low humidity (typically less than 10%). This is especially important for infrared passbands, where atmospheric emission from water vapour increases the sky brightness considerably.

IRCAM uses an InSb detector array manufactured by the Santa Barbara Research Corporation which consists of 62×58 pixels. Unlike an optical CCD, where pixels are read in columns, each pixel in the array is read separately, the detector becoming progressively de-biased as light is gathered. No bleeding occurs at saturation. Three different pixel scales are possible with IRCAM: $0\farcs62$, $1\farcs24$ and $2\farcs48$ pixel^{-1}; the $1\farcs24$ pixel^{-1} mode was used for the bulk of this work and resulted in a field of view of approximately one square arcminute.

The background in infrared passbands is considerably brighter than that in the optical: a typical value at Mauna Kea is μ_K =12.5 mag arcsec^{-2}, compared to about μ_V =22 mag arcsec^{-2} in the optical (Glazebrook 1991). For this reason, a background

limited regime is rapidly attained and short exposure times are required to ensure that the detector does not saturate. It is therefore necessary to break each exposure into several shorter ones (called "coadds"), which will then automatically be combined to form a single image. An ideal exposure time will be such that the background fills the detector wells to $\sim 2/3$ of their capacity, thus leaving enough dynamic range for the faint objects while avoiding saturation. Typical coadds in the $1\farcs24$ pixel^{-1} regime have a duration of ~ 20 seconds.

3.3.2 Reduction of IRCAM Images

The total signal obtained from IRCAM is the addition of the following components:

(i) *Dark Current:* due to thermal emission which is quite significant with infrared detectors. In IRCAM the dark current is of the order of 100 e^-pixel^{-1}s^{-1}.
(ii) *Signal* from object + background. The quantum efficiency is $\sim 80\%$.

The total signal returned by the above components is in the form of data numbers (DN), with a typical gain of 30 e^-/DN. Note the absence of a bias signal, due to the non-destructive read-out scheme of IRCAM.

The various procedures involved in reducing IRCAM frames are described in the sections that follow. Reductions were carried out on the Durham STARLINK node, using purpose-written software in addition to standard packages.

a) Linearization.

A correction has to be applied which compensates for the slight non-linearity of the array, particularly as one reaches high counts. The correction is of no more than a few percent and only becomes significant near saturation. No variation with time is observed. Data

are linearized by UKIRT staff after each night.

b) Dark subtraction.

The dark current variation throughout the night can be important on a timescale of a few hours, so it is necessary to take dark exposures every 2-3 hours. Dark exposures are simply frames taken with the same exposure times as the data, but with blank filters. These are subtracted from all data frames, the output frame being scaled to counts per second.

c) Removal of bad pixels.

Bad pixels are usually those with either a very high dark current or a very low quantum efficiency. No more than about 20 of the 3596 pixels of IRCAM are defective, and in particular the central $\sim 30 \times 30$ region is free from bad pixels. The bad pixels present in our frames were removed and replaced by the median of their surrounding pixels, although this is not critical in our case since several dis-registered frames are medianed together, as described below.

d) Flatfielding.

Flatfielding removes variations in response across the detector. The "conventional" method of flatfielding is to image a blank field near that of the target, with the same coadd time. Although high accuracies can be obtained with this method (typically 7 parts in 10^5 for a 5000 s exposure; Aragón-Salamanca 1991), the obvious drawback is that it reduces the available time for on-source exposures.

An alternative method of flatfielding is the "in-field dithering technique", which has been shown to produce optimal flatfields (better than 3 parts in 10^5). The method is described by Cowie *et al.* (1990), who pioneered its use in the infrared. The technique consists

of obtaining several dis-registered exposures of the target, each displaced by a small amount (e.g. 5 arcseconds). Flatfield frames are then obtained by median-filtering the dis-registered exposures. Each individual frame is flatfielded using a median consisting of a number of frames either side of it. The timescale for sky variations in the K band at Mauna Kea is of the order of 10-15 minutes, so that for an 80 second exposure (e.g. one consisting of 4 coadds of 20 s each), a suitable flatfield can be constructed using 8 frames which will be well matched to the current sky structure. Each one of the flatfields is then normalized to unity, and the individual object frames divided by their relevant flatfield frame.

There are two important requirements which make a dataset suitable for this flatfielding technique: the field should not be overcrowded, as substantial sky areas are needed between the objects, and it is necessary to have a suitably bright object in each individual 80 second frame whose centroid can be used for registration of the frames. In our case the QSOs themselves provide the ideal object for registration, as they are clearly detected in individual frames without being saturated.

The time savings introduced by this flatfielding technique have paved the way for very deep integrations. By achieving better signal-to-noise for equal exposure times, we also come closer to theoretical performance. We shall see in section 3.4.2 that a 3σ detection limit of $\sim$ 20.4 is reached in $\sim$ 15 000 seconds.

e) Coadding frames.

Once flatfielded, frames are registered and normalized to DN/sec. The QSO centroid in each frame is measured, and all the registered frames are then normalized to a common sky value and median-combined, giving the QSO image for each night. Finally, the total image of a given field (of the order of 15000 s) is obtained by adding the individual nights'

images weighted by their exposure times. The absence of clouds in any of the exposures and the fact that atmospheric extinction is less significant in the K band meant that it was not necessary to scale the frames by their signal.

The total exposure time for each QSO is given in table 3.2.

f) Standard Stars.

Exposures of standard stars were taken for absolute photometric calibration (see section 3.4.1). The stars are relatively bright ($\sim 7^{th}$ magnitude), and therefore when imaging standards the telescope was defocussed to avoid saturation, which would otherwise occur even at the shortest possible exposure times. Two adjacent frames with the same exposure (145 ms) were usually sufficient for flatfielding, which is not critical at such bright magnitudes.

3.4 PHOTOMETRY

3.4.1 Calculation of Zero-Points

Photometry of each individual object in our QSO fields was performed inside an aperture of 5.″0 diameter, the sky being estimated locally within similar apertures. Zero-point offsets were obtained for each night by imaging standard stars from the list of Elias *et al.* (1982). Tests were carried out between different nights to verify the consistency of the zero-points.

No correction has been made for Galactic extinction; in the K-band its value is only

$\sim$ 10% of that in optical passbands (Glazebrook 1991), and none of our selected QSOs have $|b| < 30°$.

3.4.2 Completeness of the Sample

Catalogues of object positions and magnitudes in each of the 11 QSO fields were compiled and edited to include only those objects within the magnitude limit of each field. 3σ cut-off values were calculated from plots of K-magnitude vs. error. Little variation is observed between different fields, as illustrated in figure 3.2. For most 15000 s exposures, the limiting magnitudes were in the range $K = 20.3 \pm 0.1$. One QSO, Q1331+170, was imaged for a total of 26000 s, reaching a depth of $K = 20.6$. This will be further discussed in chapter 5. The limiting magnitude of each field is given in table 3.2.

3.4.3 Photometry of Objects Close to the QSO

For those objects within a small angular distance from the QSO, a point-spread-function (PSF) subtraction technique was applied in order to remove QSO contamination and thus improve the accuracy of the measured magnitudes. The technique consists of rotating the frame by 90 or 180° about the QSO centroid and subtracting it from an identical but unrotated frame. This should eliminate the QSO, provided it has a symmetrical profile. PSF subtraction is usually done by subtracting the profile of a star scaled to the intensity of the object to be eliminated, but due to the small field of IRCAM it was not always possible to find a suitable star in the field.

The magnitudes obtained were compared with those obtained by changing the sampling scale, centroids and rotation angles. They are reproducible to within $0^m.25$.

Table 3.2. Exposure times and limiting magnitudes.

QSO	Exposure (s)	K_{lim}
Q0013−003	14850	20.3
Q0151+048	20748	20.2
B0215+015	15480	20.3
Q0237−232	15030	20.2
Q0421+016	12780	20.2
Q0424−131	13760	20.2
Q0836+195	15840	20.4
Q0854+191	15360	20.2
Q1329+412	15760	20.3
Q1331+170	25920	20.6
Q2044−168	15660	20.2

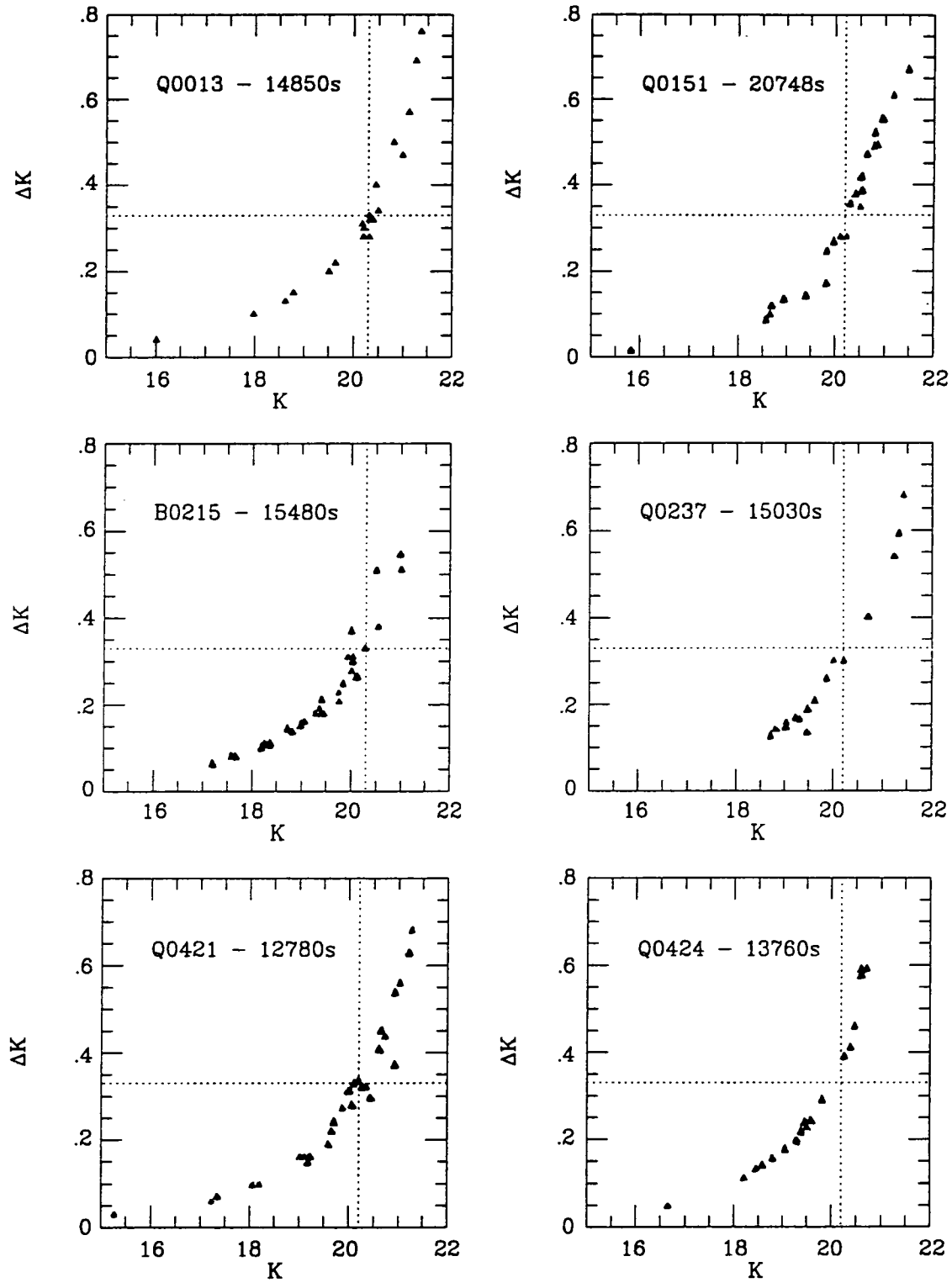

Figure 3.2. Plots of K-magnitude vs. error. The 3σ cutoff values for each field are indicated by dotted lines.

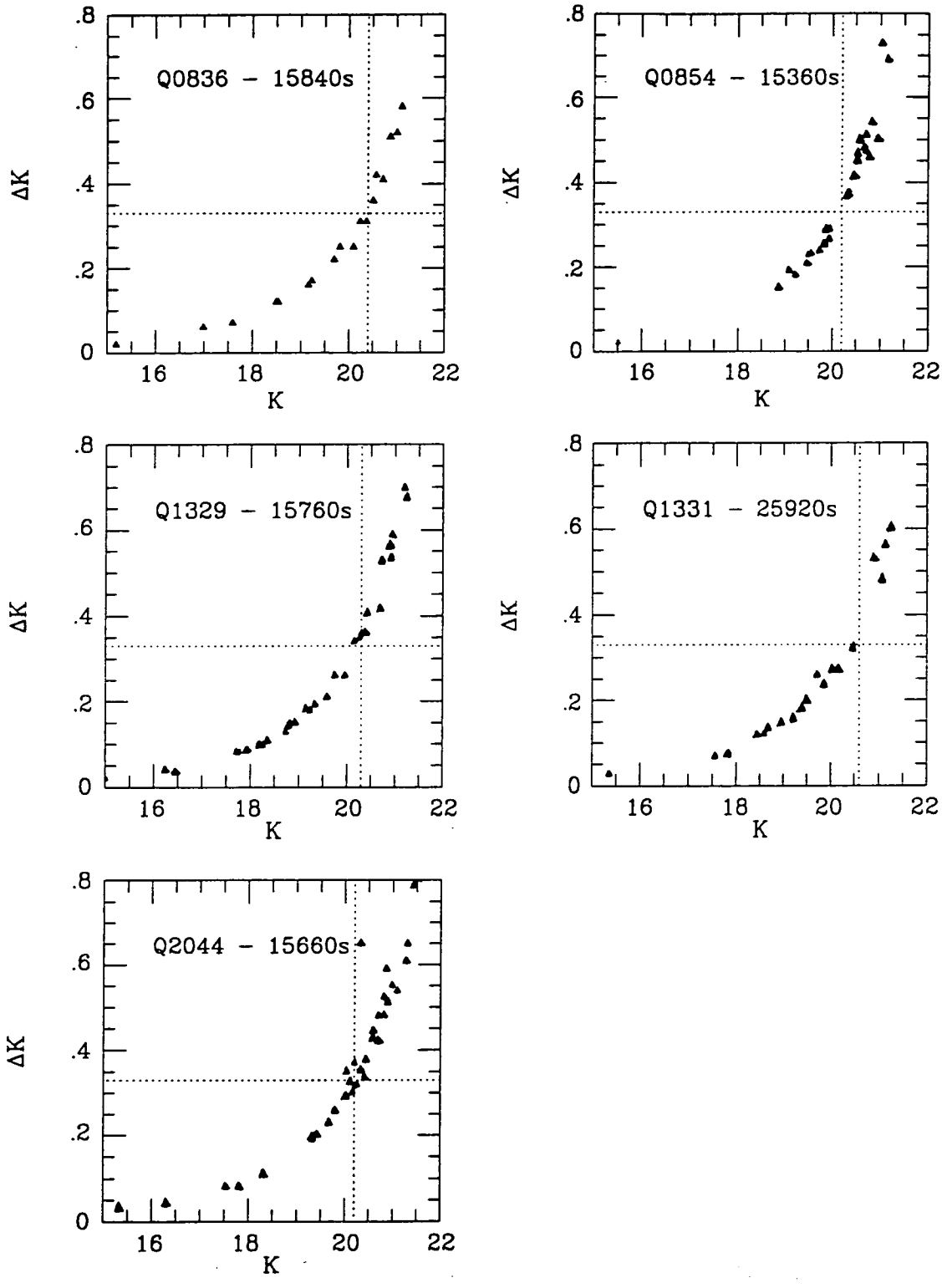

Figure 3.2. (Continued).

3.5 OPTICAL DATA

In section 3.2 we have discussed the importance of detecting galaxies in the infrared to bypass unwanted selection effects. However, the colours of a galaxy are equally important if we are to obtain any more than just a measure if its underlying luminosity. Given our absorber redshifts ($1 \leq z \leq 2$), optical-infrared colours will provide us with a measure of the galaxies' rest-frame uv-optical colours, thus yielding information on their evolutionary status, i.e. on whether the galaxies are dominated mainly by young, hot stars or by older stellar populations.

A subset of four QSOs has been imaged in the R and I bands in June 1991 by R. S. Ellis and J. A. Bergeron on the 3.6m Canada-France-Hawaii Telescope (CFHT). Details of the observations are given in table 3.3.

Images were obtained with the prime-focus camera FOCAM and the 640 × 1024 RCA2 CCD. A pixel scale of $0.''21$ pixel^{-1} resulted in a field of view of $\sim 2'' \times 3''$. Filters used were standard R (central wavelength 6490Å, bandwidth 1275Å) and I (8320, 1950).

3.5.1 Reduction Procedures

All optical images were reduced using standard IRAF software. A summary of reduction procedures is given below.

The bias was subtracted in the following way: several bias frames were taken at the beginning and end of each night and were medianed into a single master bias. The mean value of the overscan region was then subtracted from this bias frame, thus removing the constant voltage offset. The master bias was then subtracted from each data frame and,

Table 3.3. CFHT Observations.

QSO	R exposure (s)	R_{lim}	I exposure (s)	I_{lim}
Q0013−004	6000	24.5	6000	23.0
Q1329+412	4800	24.5	4800	23.0
Q1331+170	4800	24.5	9600	23.0
Q2044−168	4800	24.5	9600	23.0

in order to remove any possible variation of the bias with time (which might occur due to e.g. changes in detector temperature), the mean of the overscan of each individual frame was also subtracted.

Several dome and sky flatfields were constructed and tests were carried out to determine which one best removed the large-scale variations. The flatfields adopted were those constructed by medianing all the 20-minute exposures in each filter after normalising them to unity. Each data frame was then divided by the normalised flatfield and rescaled to its original background value.

Once flatfielded, individual exposures of a given QSO were aligned by offsetting with reference to several bright stars in the field, after which they were medianed together to produce a single image per QSO in each passband.

3.5.2 *I* Band Fringes

A considerable problem when obtaining images at longer wavelengths is the existence of interference patterns which produce a fringing effect on the images. The interference is caused by reflection of incoming monochromatic light on the internal surface of the CCD coating and occurs when the thickness of the chip is comparable to the wavelength of the light, as is usually the case in the *I* band.

Although noticeably strong in the individual *I* frames, the fringes tended to smooth out when the images were combined, producing a much less significant effect in the medianed images (typical variations were of the order of 1-2σ below/above sky). Besides, fringes appeared to be localised in certain parts of the frames and only in one case (Q2044−168) were they significant in the 30″ region around the QSO.

3.5.3 Optical Photometry

Zero-points were measured by imaging standard stars in the Ser1 field (Tyson 1988b), and aperture photometry performed in a way similar to that described in section 3.4. The limiting magnitudes were calculated in the same way as those of the K-band data and are given in table 3.3.

For those objects close to the QSO line-of-sight, PSF subtraction (see §3.4.3) was attempted but did not produce adequate results, despite the good resolution available. This was due to the fact that the QSO was saturated in most of the individual 20-minute exposures, so that it was not possible to calculate the QSO centroid accurately. For the same reason it was not possible to scale and subtract the profile of a field star although, contrary to the K-band case, several such stars would have been available within our fields. The magnitudes of close-by objects were therefore measured in the presence of the QSO, with the aperture centre slightly offset from the object's centre so as to avoid QSO contamination as much as possible.

3.6 SUMMARY

In this chapter we have described the observations carried out and the data-reduction procedures, with special emphasis being given to the K-band data which constitutes the main body of this work. We have obtained in total 11 deep images reaching at least $K = 20.2$, with one field in particular having been imaged for over 25,000 seconds to a depth of $K = 20.6$. We also have a subsample of four QSOs imaged in R and I, reaching

$R = 24.5$ and $I = 23.0$. Contour plots of our fields are shown in Figure 3.3. We now present in chapter 4 the results obtained and discuss their implications.

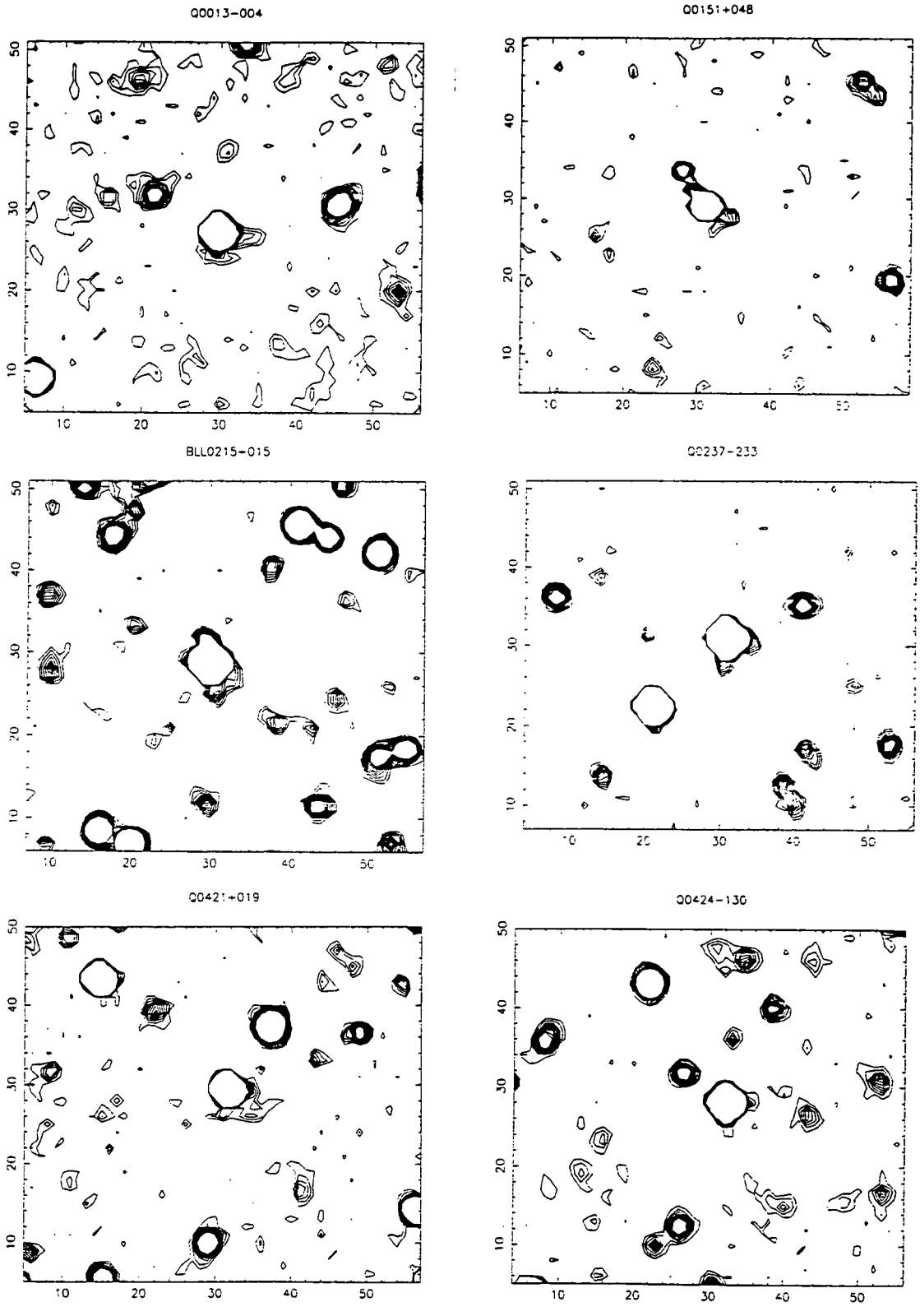

Figure 3.3. Contour plots of our fields in the K-band. North is at the top and East at the left, and each image is approximately one square arcmin. The QSO lies at the centre of each field.

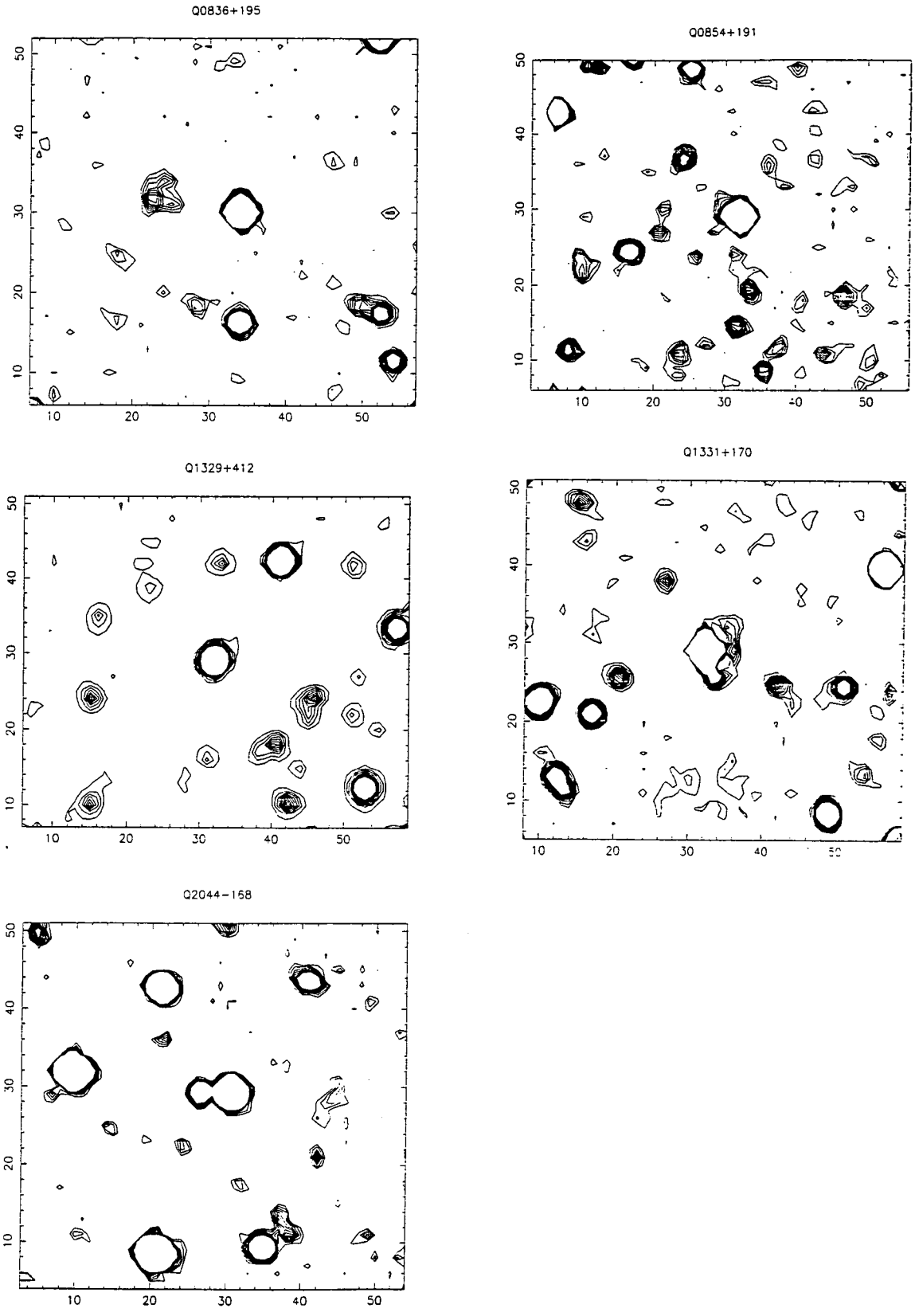

Figure 3.3. (Continued).

4 ANALYSIS OF 11 QSO FIELDS

4.1 INTRODUCTION

In this chapter we describe the analysis and conclusions drawn from our data. We have set out to detect a population of field galaxies at redshifts $z \gtrsim 1$, in the hope of obtaining clues about the evolutionary status of normal galaxies at a time close to their epoch of formation. In face of the difficulties involved in detecting such galaxies, due to their faint apparent magnitudes, we use background QSOs as indicators, the presence of lower redshift absorption lines in their spectra pointing to the existence of gas along the line of sight.

With this aim we have obtained deep infrared images of the regions around 11 QSOs whose spectra were known to be rich in C IV absorption features. Our exposures reach sufficiently deep limits to detect unevolved L^* galaxies at $z \simeq 2$. We have also obtained R and I optical images for a subsample of our QSOs. These data combined should provide both a measure of the underlying luminosity of the objects detected (since at the redshifts concerned the infrared K band samples the optical region of a galaxy's spectrum, and is thus more representative of the galaxy's underlying mass) and an indication of the evolutionary stage of the galaxies, via their optical-infrared colours.

Before measuring these properties, however, we need to investigate the possible origin of the objects detected. We thus proceed in the following way: we produce catalogues of all objects detected to our K limit in each QSO field, and compare the number of detected objects with that predicted by independent measurements of random fields. In this process we coadd all the 11 catalogues in order to obtain higher signal to noise. A strong concentration of excess sources is detected within a small angular region of the QSOs. We investigate in detail the possibility that this detected excess is related to lower redshift Mg II absorbers or to the QSO itself, but find both of these hypotheses unlikely in the light of previous studies of confirmed Mg II absorbers.

Having concluded, therefore, that the objects are most likely to be associated with the C IV systems in the range $1.2 \leq z \leq 2.0$, we examine the properties of the candidate absorbers, assuming them to be at the C IV redshifts. We discuss their impact parameter distribution, absolute K magnitudes and optical-infrared colours, and discuss the implications of our results.

4.2 THE PHOTOMETRIC CATALOGUES

Photometric catalogues were compiled for each of the 11 QSO fields, containing the positions and K magnitudes of all detected sources in the frames. The catalogues were subsequently edited to include only objects brighter than the appropriate limiting magnitude as calculated in section 3.4.2. Objects less than 3.″0 or more than 27.″0 away from the QSO were also excluded. The outer limit represents the largest complete circular area in the IRCAM field, after registration of the dithered frames. The inner limit, 3.″0,

corresponds to the region inside which objects could not have been reliably detected, even after applying the QSO point-spread-function subtraction technique described in Chapter 3. The final catalogues, presented in Appendix A, give for each field the object number, x and y position in pixels, projected separation from QSO in arcseconds and K magnitude and error. For the subsequent analysis the 11 catalogues were combined into a single one, as the number of objects per field was not sufficient to allow a field-by-field analysis.

4.3 STATISTICAL SUBTRACTION OF FIELD COUNTS

To investigate the existence of any excess number of galaxies in our fields, we have compared our data to the published counts in random areas of the Hawaii Deep Survey (Cowie *et al.* 1991a), which reaches a depth of $K = 22.0$.

4.3.1 Scaling of the Counts

The field counts of Cowie *et al.* (hereafter "Cowie counts") are presented in table 4.1, binned in unit magnitude intervals in the range $17 \leq K \leq 23$. These have been corrected for incompleteness by the authors. As our limiting magnitudes varied between 20.2 and 20.6, the counts were summed up to $K = 20.0$ and $K = 21.0$ and the values for the range $20.0 \leq K \leq K_{lim}$ interpolated using a fit of the form

$$N(< K) = \frac{N(K, K + \delta K)}{\delta K \gamma \ln(10)}, \tag{4.1}$$

where

$$N(K) = n_0 10^{\gamma K},$$

with the values $\gamma = 0.35615$ and $n_0 = 1.8719 \times 10^{-3}$.

From this fit we obtain the Cowie counts averaged to our combined limiting magnitudes,

$$N_{Cowie} = 38370 \text{ Galaxies / square degree.}$$

4.3.2 Contamination from Stars

We have not attempted to discern between stars and galaxies when compiling our photometric catalogues. Cowie's counts, however, refer to galaxies only and therefore in order to compare them with our data we have added 10% to the field counts, which is equivalent to the stellar contribution estimated by Cowie *et al.* for the range $17 \leq K \leq 20$ and in agreement with the theoretical predictions of Lilly & Cowie (1986). We note that both our QSO fields and the Cowie fields have roughly the same galactic latitudes, with our $< |b| > \simeq 50° \pm 16°$.

4.3.3 Field Count Subtraction

The objects in the catalogue have been binned into annuli according to their projected distance from the QSO. The Cowie counts were scaled to the respective area of each bin and subtracted from the data, producing the result shown in figure 4.1 . In that figure, the upper panel shows the total number of objects detected in each annulus, N_{data}, superimposed on the Cowie numbers scaled to the total area (dotted line). The lower panel shows the same data in terms of the excess over the field counts, namely

Table 4.1. Cowie Field Counts.

K interval	N_{field}	ΔN_{field}
17–18	3462	900
18–19	9462	1477
19–20	22400	4032
20–21	38500	5775
21–22	74700	11205
22–23	99600	23904

$$\text{Excess} = \frac{\text{N}_{data} - \text{N}_{Cowie}}{\text{N}_{Cowie}}. \tag{4.2}$$

The errors quoted in both the counts and our data have been calculated assuming Poissonian statistics. A clear excess is observed in the innermost bin, $3\farcs0 \leq z \leq 6\farcs0$, whereas the number of sources agrees reasonably well with the field counts at larger radii. We now investigate the significance of this excess.

Overall, in the $3\farcs0 \leq r \leq 27\farcs0$ range, 124 objects are detected in the 11 fields combined (11.3 per field), compared to a total of 82 (7.4 per field) predicted by Cowie. This result in itself would not be extremely significant, given all the uncertainties involved (stellar contamination, zero-point and other systematic errors). However, we note that most of this excess arises in the region within $6\farcs0$ of the QSO, where $N_{data} = 19$ and $N_{Cowie} = 3.1 \pm 0.4$, giving a 3.25σ excess of 5.2 ± 1.6.

The good agreement of our data counts with N_{Cowie} at large radii appears to be a strong indication of the reality of the inner area excess, which only a large adjustment in the field counts – by a factor of 1.6 – could eliminate.

We now proceed to analyse the origin and properties of the objects detected, concentrating on those 19 sources detected in the $3\farcs0 \leq r \leq 6\farcs0$ annulus, which hereafter are referred to as the candidate absorbers.

4.4 ORIGIN OF THE ABSORBERS: C IV , Mg II OR QSO-RELATED?

There is no way of unequivocally establishing the nature of the absorbers other than

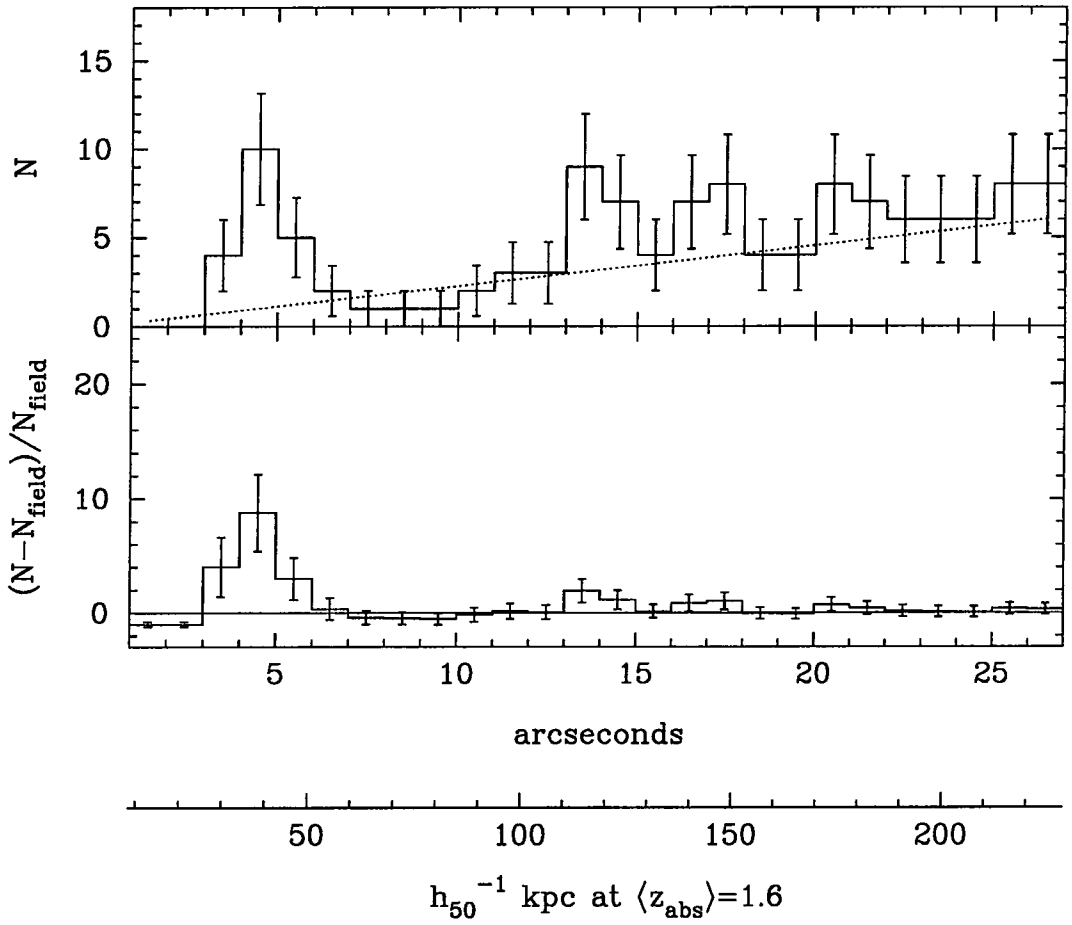

Figure 4.1 Radial distribution of excess objects around the QSO, in absolute numbers superimposed on the field counts (dotted line, upper panel) and in terms of the multiplicative excess over the field counts (lower panel). Also shown is the projected impact parameter of the sources (assuming $q_0 = 0.5$) at $z_{abs} = 1.6$, the mean absorber redshift.

to measure their redshifts. However, given the difficulties of obtaining spectroscopic confirmation at these magnitudes, we now turn to a discussion of the possible origins of the detected objects, arguing that they are *most likely* to be related to C IV systems.

4.4.1 Mg II Systems at $z < 1$

Our QSOs were originally chosen because they contained clustered C IV systems, regardless of their low redshift absorption properties. However, of the 10 QSOs with detected absorbers in the $3''.0 < r < 6''.0$ region, four have Mg II systems at $z < 1$ and it is therefore reasonable to question whether some or all of our detected galaxies are not in fact responsible for this observed Mg II absorption.

Before examining this hypothesis by looking at the candidate absorbers' magnitudes, we have tested the assumption that our QSOs have typical $z < 1$ absorption properties. This is expected to be the case since the QSOs were selected without any knowledge of those properties. We recognise however the limitations of our statistics, given the small number of QSOs and the different redshift ranges probed.

We have computed the mean number of Mg II systems observed up to a given redshift by Steidel & Sargent (1992, hereafter SS92) and compared it with the number observed in each of our sightlines. For the seven QSOs in common with their sample, we find a mean of 1.3 ± 0.7 $z_{abs} < 1$ Mg II systems per sightline, whereas the mean for the entire SS92 sample (along the same total redshift range) is 1.8 ± 0.2 systems per sightline. Thus we deduce that our QSOs have a typical number of lower-redshift Mg II systems per sightline.

A similar method to that above, giving the same qualitative result, is to compare the observed number of absorbers along our sightlines with the number predicted by the

$N(z)$ relationship and derived from the SS92 sample. The predicted number should then be more reliable since it will have been derived from a larger, homogeneous sample. At a mean redshift $< z_{abs} >= 1.2$, SS92 predict a total of ~ 8 Mg II systems per sightline. We observe 4 systems, although when converted to the same total redshift length sampled by SS92, this becomes equivalent to ~ 7 systems, thus in accordance with the number expected from $N(z)$. We conclude therefore that our selection of QSOs, based on their $z > 1$ absorption properties, still provides an unbiased sample with respect to $z < 1$ absorption properties.

An important factor that would appear to discard the Mg II hypothesis is the observed magnitudes of the candidates. The faintest absolute magnitudes of the confirmed absorbers of Bergeron & Boissé (1991, hereafter B&B) and Steidel (1993b) are respectively $L/L^*_B = 0.3$ and $L/L^*_B = 0.25$, and thus we can compare these limits with the magnitudes implied if our absorbers were placed at the Mg II redshifts. In most cases our objects would be intrinsically very faint in K, with e.g. $L/L^*_K = 0.04$ (see table 4.2), and therefore to reach B luminosities comparable to those of B&B and Steidel they would have to have unusually blue colours. We can rule this out for those objects for which we have optical magnitudes: none are extremely blue, as can be seen in figure 4.4. Furthermore, three candidate absorbers in QSOs with Mg II systems at $z < 1$ have R and I band magnitudes. These can be converted into rest-frame B magnitudes, enabling a more direct comparison with the confirmed Mg II absorbers. The R band closely matches the rest-frame B band for the QSOs with $z_{abs} = 0.45$ and 0.50, the same occurring with the I band for the QSO with $z_{abs} = 0.74$.

The rest-frame B magnitudes obtained are shown in table 4.2; the Mg II redshifts are from Sargent *et al.* (1988). Given that the faintest absorber found by Steidel has $M_B = -19.4$

and $M_B^* = -21.0$ (Loveday *et al.* 1992), we see that our absorbers would be at least 5 times less luminous than the faintest of Steidel's sample. One case however in which this argument remains invalid is that of Q1331/2, whose B magnitude would fall well within a typical Mg II absorber magnitude at $M_B = -20.4$.

From the above considerations we believe it is highly unlikely that all the excess objects detected could be explained by low redshift Mg II absorption systems. However, given the success rate of detection of absorbers in both Mg II surveys (B&B, Steidel 1993b), we might be tempted to ask where *are* our Mg II absorbers. One possibility is that they lie at very small angular separations from the QSO, in which case they cannot be easily detected in the K band ($1\farcs24$ pixel^{-1}). Preliminary results from point spread function subtraction in the I band, where the resolution is higher than in the infrared, point to the presence of at least one superimposed object in the field of Q1329+412.

The absorbers identified by Steidel have impact parameters ranging up to $80h_{50}^{-1}$ kpc. At $z = 0.27$ this corresponds to over 15 arcseconds, so that several other objects within the field but outside the $6\farcs0$ range could conceivably be the Mg II absorbers. Lanzetta & Bowen (1990) have correlated the rest-frame equivalent width of the Mg II (λ2796) line with the impact parameters of the confirmed absorbers of B&B. Applying their correlation to our QSOs allows us to calculate the predicted impact parameters of the hypothetical Mg II absorbers. It is found that most lie *outside* the $6\farcs0$ range: the angular separations predicted in this way for the four Mg II QSOs are $6\farcs5$, $16''$, $14''$and $1\farcs5$.

4.4.2 QSO-Galaxy Associations

Whilst care was taken to ensure that our sample did not contain QSOs with $z_{abs} \approx z_{em}$, there remains the possibility that the galaxies detected are physically associated with

Table 4.2. Absolute K and B magnitudes of absorbers assuming Mg II absorption redshifts.

Candidate	z_{abs} (Mg II)	M_K	L/L_K^*	M_B	L/L_B^*
Q0013/22	0.45	−21.5	0.04	−18.3	0.08
Q0013/23	0.45	−21.6	0.04	-	-
Q0854/2	0.27	−20.6	0.02	-	-
Q1329/25	0.50	−22.1	0.06	−17.8	0.05
Q1331/2	0.74	−24.3	0.48	−20.4	0.50
Q1331/31	0.74	−22.8	0.12	-	-

the QSO, either as the host galaxy (Lehnert *et al.* 1992) or as parts of larger associations. If this were to be the case then our absorbers could no longer be considered as fair representatives of normal galaxies at high redshifts, since QSO environments are believed to affect considerably the properties of surrounding galaxies, through higher-than-background UV ionisation, mass interactions and other phenomena (see e.g. Yee 1988). Furthermore, radio-loud QSOs tend to have denser environments than radio-quiet ones (Yee and Green 1987), and eight of our 11 QSOs show signs of radio emission (Hewitt & Burbidge 1987). Of the three QSOs in the sample without evidence for radio emission, Q0013−004 and Q1329+412 both have one absorber each, while Q0151+048 has three absorbers detected within our 6.″0 radius. If radio activity were to bear an influence on the number of absorbers detected, then the excess should increase when considering only radio-loud QSOs. However, this turns out not to be the case: with our sample reduced to 8 radio-loud QSOs, we find our total number of candidates in the innermost bin equal to 14, for a background of 2.25 objects. The excess (as defined in equation 4.2) is therefore 5.2, i.e. *the same as for the whole sample.*

Yee and Green (1987) have quantified the amount and scale of clustering around lower redshift QSOs ($z < 1$) in terms of the galaxy-QSO spatial correlation function amplitude, B_{gq}. Based on their mean value of B_{gq}, we have computed the expected number of galaxies associated with our QSOs within the $3.''0 < r < 6.''0$ area. We have used the parameters of Mobasher *et al.* (1992) to integrate a K-band luminosity function for each of our QSOs to $M_{K_{lim}}$ at the appropriate redshift ($< z_{em} > \simeq 2.0$). Using a value for B_{gq} of 540 (a generous estimate of the correlation amplitude, corresponding to an Abell class $0-1$ cluster) and assuming no luminosity evolution of the galaxies, the predicted number of galaxies associated with each QSO ranges between 0.04 and 0.06. As we find an average of 1.4 galaxies per field after background subtraction, it thus appears unlikely

that the excess can be explained in terms of QSO-galaxy clustering. Even assuming an extreme scenario, with $B_{gq} = 1000$ and a two magnitude brightening due to luminosity evolution of the galaxies, the predicted number of associated galaxies would be no greater than 0.20 per field.

We now ask what value of B_{gq} would be implied if our excess galaxies were indeed clustered around the QSOs. Assuming a mean emission redshift of 2.0, the clustering would imply $B_{gq} = 14250$ or, in the $\Delta M_K^* = 2$ case described above, $B_{gq} = 6800$. In their sample of 31 QSOs, Yee and Green find that only six have $B_{gq} > 500$.

All the above calculations were made assuming $H_o = 50$ kms^{-1}mpc^{-1} and $q_o = 0.5$. Changing the value of q_o to 0.0 would not alter the conclusions significantly: in the first case ($B_{gq} = 540.0$, no evolution) the mean predicted number becomes 0.02 and in the evolutionary case 0.30. The values of the correlation function required in a $q_o = 0.0$ Universe would thus rise to 4885 and 27400 respectively.

We might ask whether it is reasonable to establish a comparison between our high-redshift QSOs and those of Yee and Green, which all have $z \leq 0.65$. Indeed their values of B_{gq} show a tendency to increase with redshift (which they interpret as evolution in the QSO environments), but the amount of evolution required to match our excess number of galaxies still appears to be too high to explain our detections in terms of QSO-galaxy clustering. We stress also that, besides the discrepancy between the number of absorbers detected and the number predicted by the correlation function, the clustering scale of our absorbers (typically 30-40 kpc, see section 4.5.2) is also much smaller than that found by Yee & Green (1987), where the galaxies (although at lower redshifts) tend to cluster around the QSOs on scales of a few hundred kpc.

4.4.3 Conclusions

In the above discussion we have examined the possibilities that our candidate absorbers are either associated with lower redshift Mg II systems or with the QSO. We have first demonstrated that selecting QSOs with clustered C IV systems does not entail a bias in the number of Mg II systems present along the lines of sight. The absolute magnitudes of the candidates, assuming them to be at the Mg II redshifts, offer a compelling argument against this hypothesis, in all cases but one. However, we do not eliminate this object from our sample, as we have no similar information on the rest of the candidates. Combining this evidence with the small angular region within which our excess is detected, which leaves open the hypothesis that the Mg II absorbers are at larger (or smaller) angular separations, we conclude that there is no evidence linking our candidate absorbers with $z < 1$ Mg II systems.

Similarly, analysis of the clustering properties of galaxies aroud QSOs at lower redshifts indicates that the scale and amplitude of our excess cannot reasonably be ascribed to QSO-galaxy associations. We thus conclude that the detected candidates are most likely to be associated with the C IV absorption systems. In the following sections we derive the intrinsic properties of the candidates, assuming them to be at the C IV redshifts.

4.5 INTRINSIC PROPERTIES OF THE ABSORBERS

4.5.1 The Mean Absorption Redshift of Each QSO

We have seen in section 2.5 that, in the absence of spectral confirmation, we are con-

strained to assume that our absorbers are indeed at the C IV redshifts. Now that this assumption has been strengthened by the arguments presented in the previous section, we proceed to calculate the mean absorption redshift for each QSO. These values will be used when inferring distance-related properties of the absorbers such as impact parameters and absolute magnitudes.

To calculate the mean absorption redshifts, each C IV absorption system in a given QSO is weighted by its total rest equivalent width. Calculated in this way, the mean absorption redshift of the whole sample is $< z_{abs} >= 1.64$. Individual values for each field are given in table 4.3, with the number of C IV doublets within each system indicated in brackets.

4.5.2 Impact Parameters and Apparent Magnitudes

The distribution of linear impact parameters of the absorbers (fig.4.2) is strongly peaked between 30 and $40h_{50}^{-1}$ kpc ($q_o = 0.5$) or around $55h_{50}^{-1}$ kpc for $q_o = 0.0$. The mean impact parameter of the $z \simeq 0.5$ absorbers of Bergeron & Boissé (1991) was, similarly, $\sim 50h_{50}^{-1}$ kpc for $q_o = 0.0$ (see section 2.3.1). Assuming that both Mg II and C IV systems are representative of the same regions of galactic halos, then the similarity between our impact parameters and those of the confirmed Mg II absorbers of B&B and Steidel (1993b) would seem to imply that no significant evolution in galactic halo size has taken place between $z \simeq 1.6$ and $z \simeq 0.5$.

No significant correlation is found between the absorbers' absolute magnitudes and impact parameters, contrary to Steidel (1993b) where the brighter absorbers are usually detected at larger angular separations. Similarly, we find no correlation between the mean equivalent width of the C IV (λ1548) line along a given sightline and the impact parameter of the corresponding candidate absorber.

Table 4.3. Clustered C IV absorption systems and mean absorption redshifts. Numbers in brackets indicate the number of doublets seen in each system.

QSO	z_{abs}(n)	$< z_{abs} >$
Q0013−004	1.973(4)	1.85
Q0151+048	1.657(4)	1.67
BLL0215+015	1.549(3),1.649(7)	1.51
Q0237−232	1.599(3),1.657(4),1.673(4)	1.62
Q0421+016	1.638(3)	1.65
Q0424−131	1.560(3)	1.65
Q0836+195	1.424(2+)	1.41
Q0854+191	1.297(3),1.353(3),1.734(2+)	1.49
Q1329+412	1.836(3)	1.68
Q1331+170	1.776(3)	1.74
Q2044−168	1.733(3+)	1.79

Table 4.4. Apparent magnitudes and impact parameters of the absorbers.

Object	$K \pm \Delta K$	$D(")$	$D_{q_0=0.5}$(kpc)	$D_{q_0=0.0}$(kpc)
Q0013/22	20.18 ± 0.28	3.6	30	46
Q0013/23	20.07 ± 0.30	5.5	46	70
Q0151/2	19.26 ± 0.14	3.5	30	44
Q0151/4	18.52 ± 0.10	4.5	38	56
Q0151/5	19.70 ± 0.17	3.9	33	49
BLL0215/2	18.94 ± 0.16	4.8	41	59
BLL0215/3	19.62 ± 0.21	4.5	38	55
BLL0215/4	19.33 ± 0.18	4.0	34	49
Q0237/2	19.17 ± 0.17	4.1	35	51
Q0237/3	18.89 ± 0.15	4.6	39	57
Q0421/2	19.45 ± 0.19	5.3	45	66
Q0421/3	19.10 ± 0.16	4.4	37	55
Q0421/4	19.03 ± 0.15	4.4	37	55
Q0424/3	19.50 ± 0.23	5.8	49	72
Q0854/2	19.90 ± 0.29	3.9	33	48
Q1329/25	19.75 ± 0.26	4.0	34	50
Q1331/2	18.57 ± 0.12	4.3	36	54
Q1331/31	20.03 ± 0.27	6.0	50	76
Q2044/2	17.66 ± 0.08	5.2	43	66

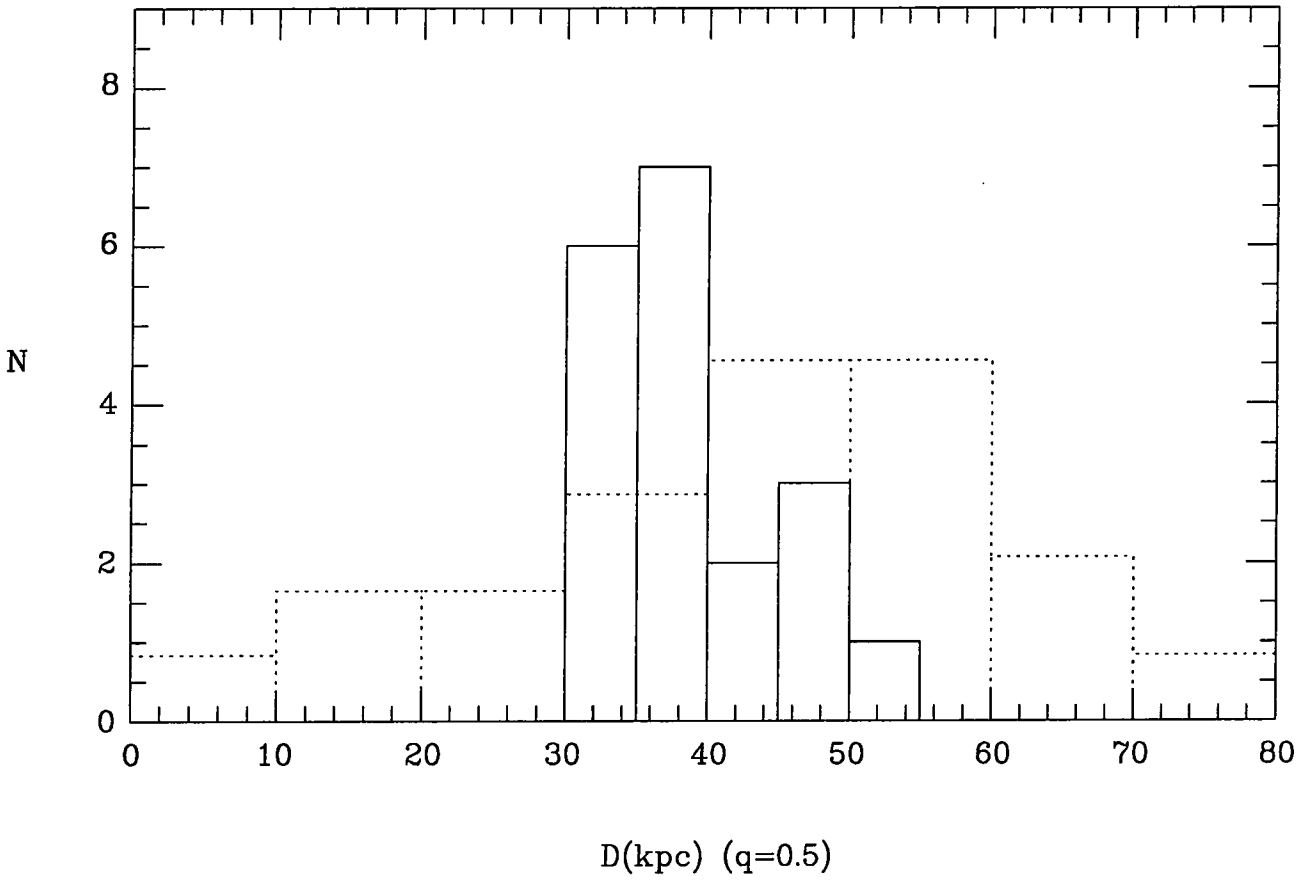

Figure 4.2 Impact Parameter distribution of Candidate Absorbers. The distribution of Steidel (1993a) is shown for comparison (dotted histogram).

4.5.3 Absolute K Magnitudes

To calculate the absolute magnitudes of the absorbers it is necessary first to measure their luminosity distance, d_L. An object at a redshift z has a luminosity distance given by

$$d_L = \frac{c}{H_o q_o^2}[q_o z + (q_o - 1)(\sqrt{1 + 2q_o z} - 1)]. \tag{4.3}$$

An equivalent expression for d_L in the particular case where $q_o = 0$ is (Glazebrook 1991):

$$d_L = \frac{cz}{2H_o}(2 + z). \tag{4.4}$$

The absolute magnitude of a galaxy, M, is then obtained from the distance modulus,

$$m - M = 5\log(d_L) + k(z) + E(z), \tag{4.5}$$

where m is the galaxy's apparent magnitude, d_L is the *Luminosity Distance* in units of 10 kpc and $K(z)$ and $E(z)$ are respectively the k-correction and an evolutionary correction. The notation used for magnitudes hereafter is K, R and I for apparent magnitudes, and M_K, M_R and M_I for the corresponding absolute magnitudes. The k-correction applied to the absolute K magnitudes in subsequent calculations was $k = -0.7$ (Aragón-Salamanca *et al.* 1992). This value remains constant over our absorber redshift range. Zero luminosity evolution is assumed throughout.

The absolute magnitudes of the absorbers are plotted in figure 4.3. Also shown is the value of M_K^*, as determined locally by Mobasher *et al.* (1992). Individual M_K values for the absorbers are given in table 4.5.

Table 4.5. Absolute K magnitudes and luminosities of the absorbers.

Object	$M_K(q_0 = 0.5)$	$L/L^*_K(q_0 = 0.5)$	$M_K(q_0 = 0.0)$	$L/L^*_K(q_0 = 0.0)$
Q0013/22	−24.84	0.79	−25.77	1.85
Q0013/23	−24.95	0.87	−25.88	2.05
Q0151/2	−25.51	1.46	−26.36	3.19
Q0151/4	−26.25	2.89	−27.10	6.32
Q0151/5	−25.07	0.97	−25.92	2.13
BLL0215/2	−25.59	1.57	−26.37	3.21
BLL0215/3	−24.91	0.84	−25.69	1.71
BLL0215/4	−25.20	1.09	−25.98	2.24
Q0237/2	−25.53	1.48	−26.36	3.18
Q0237/3	−25.81	1.92	−26.64	4.11
Q0421/2	−25.29	1.19	−26.13	2.59
Q0421/3	−25.64	1.65	−26.48	3.57
Q0421/4	−25.71	1.76	−26.55	3.81
Q0424/3	−25.24	1.14	−26.08	2.47
Q0854/2	−24.59	0.63	−25.36	1.28
Q1329/25	−25.05	0.96	−25.91	2.11
Q1331/2	−26.30	3.02	−27.18	6.80
Q1331/31	−24.84	0.79	−25.72	1.77
Q2044/2	−27.28	7.45	−28.18	17.09

The mean absolute magnitude of the sample is $< M_K >= -25.5 \pm 0.6$, thus agreeing with the present-day M_K^* within the errors. Our derived luminosity function (LF) matches that of Mobasher *et al.* with an arbitrary normalisation. Thus the *shape* of our LF appears to imply no luminosity evolution. Due to passive evolution, however, one would predict that galaxies at $z \simeq 1.6$ should be considerably brighter than their present-day counterparts. For this reason our candidate absorbers may be in fact slightly *under*luminous compared to other sources at similar redshifts.

The high normalisation factor obtained from our LF implies a significant decrease in the volume density of galaxies from $z \simeq 1.6$ to the present epoch. This could give partial support to the merging models of galaxy evolution (see chapter 1), whereby a number of sub-units have merged to form the observed present-day luminous galaxies (although in this case we would expect our galaxies to be considerably fainter). Our large number density may also be due in part to a selection effect: by choosing QSOs with clustered C IV systems we may have biased our lines of sight, e.g. they may be more likely to pass through clusters and therefore not be representative of random areas of sky. Clearly a combination of these factors (merging *and* selection effect) could be taking place.

4.5.4 Optical-Infrared Colours of the Sample

For the QSOs for which we have optical data, we present in table 4.6 their R and I magnitudes. The $R - K$ colours of our sample range between 1.3 and 3.8, with an additional object (Q0013/23) not detected in R, whose K magnitude ($K = 20.2$) would imply $(R - K) > 4.8$. The colours are shown in figure 4.4, superimposed on those of the field galaxies of Cowie *et al.* (1991a). Note that none of our absorbers have very extreme colours.

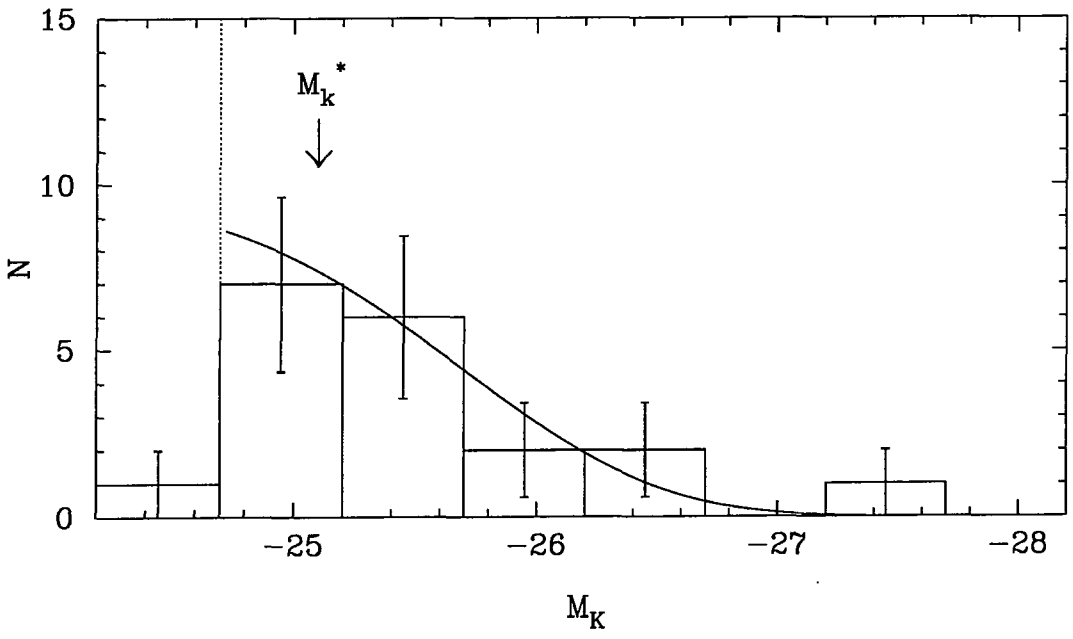

Figure 4.3 Luminosity function of candidate absorbers. The arrow shows the present-day value of M_K^* and the dotted line shows the limit at which our sample becomes incomplete. The curve represents the luminosity function of Mobasher *et al.* (1992) normalised to our total number of absorbers.

Table 4.6. Optical R and I Magnitudes.

Object	$R \pm \Delta R$	$I \pm \Delta I$
Q0013/22	23.34 ± 0.15	21.59 ± 0.08
Q0013/23	-	-
Q0151/2	20.71	18.86 ± 0.01
Q0151/4	21.94	21.17 ± 0.07
Q0151/5	23.22	22.06 ± 0.18
Q1329/25	23.75 ± 0.15	21.33 ± 0.04
Q1331/2	23.15 ± 0.15	21.75 ± 0.11
Q1331/31	23.20 ± 0.11	-
Q2044/2	21.01 ± 0.02	19.33 ± 0.01

Note: For Q0151+048, R magnitudes are from Meylan (1990) and I magnitudes from Aragón-Salamanca (1991).

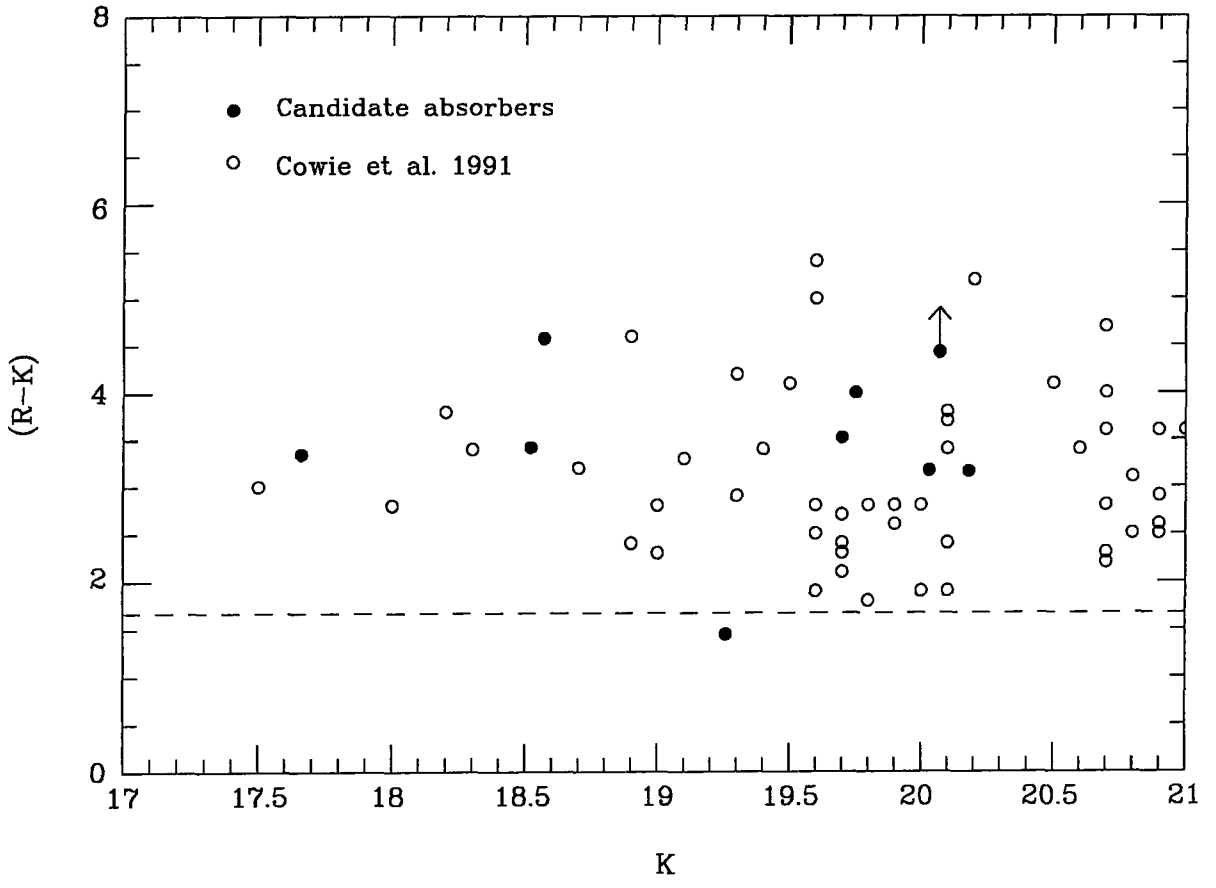

Figure 4.4 $R - K$ Colours of Candidate Absorbers and Field Galaxies of Cowie *et al.* (1991a). The dashed line is indicative of a flat spectrum source.

4.5.5 Summary

Inspection of the properties of our 19 candidate absorbers shows that they have absolute K magnitudes typical of present-day L^* galaxies. Our candidates' mean K-band luminosity is in agreement with the locally derived M_K^*, although models suggest that at our redshifts galaxies could be up to 2 magnitudes brighter than their present-day counterparts. This would also imply, however, that the galaxies should have been considerably bluer in the past. Our candidates show normal $R-K$ colours, typical of those observed in field surveys. At $z \simeq 1.6$, such colours appear to be indicative of mid-to-late type spirals. This result, combined with the implied M_K^* of our galaxies, indicates that our absorbers are most likely to be slowly evolving luminous galaxies.

No evidence was found for a possible correlation between the impact parameters of the candidate absorbers and their absolute magnitudes or the rest-frame equivalent width of their strongest C IV system. Their linear impact parameters are in the range $30-55h_{50}^{-1}$ kpc, suggesting that the galaxies are members of small, compact groups.

5 CONCLUSIONS AND FUTURE PROSPECTS

In this chapter we summarise the main results of this work, outlining the principal properties of our candidate absorbers. We then discuss the possibility of obtaining spectroscopic confirmation of the absorbers' redshifts and a strategy for extending this work to higher redshifts.

5.1 Summary of Results and Conclusions

We have obtained deep infrared images of 11 QSO fields, in a search for the objects responsible for the C IV absorption systems observed in QSO spectra. We have found a statistically significant excess of sources when compared to the expected number of objects in the field. These excess objects appear to be tightly concentrated within $\approx 6\farcs0$ of the QSOs. Within this region 19 objects are found, while the prediction of the field counts is $\approx$ 3 objects.

We have examined the possibility that the objects detected arise either at low redshifts (e.g. as Mg II absorbers) or at the QSO redshifts, as parts of QSO-galaxy associations. These hypotheses are ruled out through comparisons with previous work, on the basis of the observed magnitudes of the objects and their clustering amplitude and scale. We

thus conclude that the objects detected are most likely to be associated with the C IV systems seen in the $1.2 \lesssim z_{abs} \lesssim 2.0$ region.

The photometric properties of the excess objects point to luminous galaxies whith colours comparable to those of the field population and a mean K luminosity similar to the present-day L_K^*. The luminosity function of our candidates is similar in shape – but not in normalisation – to the present-day luminosity function. Their colours are relatively blue, typical of spiral galaxies of type Sbc or later.

All the significant excess is detected within 6.″0 of the QSOs, which at the mean absorber redshift corresponds to $\approx 60 h_{50}^{-1}$ kpc. The impact parameter distribution of the absorbers reaches a peak between $30 h_{50}^{-1}$ and $40 h_{50}^{-1}$ kpc. This is comparable to the impact parameters derived from previous studies of Mg II absorbers, thus ruling out substantial evolution in halo sizes between $z \simeq 1.6$ and $z \simeq 0.5$.

Finally, the high density of objects within the small volume implied by the angular separation of the absorbers shows that the absorbers are most likely to be members of small groups. This would therefore support the so-called "merging models" of galaxy evolution, which suggest a substantial change in the volume density of galaxies from redshifts $z \simeq 1.5$ to the present epoch. The very high number density when compared to the present-day luminosity function, however, indicates that a selection effect might be taking place, our lines of sight being biased perhaps by the choice of QSOs with clustered absorption systems.

Irrespective of the conclusions pertaining to the galaxies' properties and their evolutionary status, this survey has proved that deep infrared imaging is capable of detecting normal galaxies at high redshifts, provided a suitable strategy is used for locating such galaxies.

5.2 Future Prospects: Spectroscopic Confirmation and Extension to Higher Redshifts

Clearly, obtaining spectra of our candidate absorbers would be the only unequivocal way of confirming their association with the C IV systems. A trial spectroscopic run was carried out in August 1992 (observers R.S. Ellis and A. Aragón-Salamanca) using the LDSS-2 spectrograph on the 4.2m William Herschel Telescope in an attempt to secure redshifts for candidates in the fields of Q0013−004 and Q2044−168. However, an 18,000 second exposure of Q0013−004 did not provide the signal to noise necessary to secure redshifts. The candidate absorbers had magnitudes in the range $22.5 \leq R \leq 23.7$. Note that redshift determination in this case is made particularly difficult by the fact that no strong emission lines fall in the optical window for the redshift range of our expected absorbers. We might therefore only be able to place lower and upper limits on redshift, based on the presence/absence of the [O II] and Ly α lines.

One of the QSOs in our sample, Q1331+170, has been imaged for 26,000 seconds in an attempt to demonstrate the feasibility of extending our survey to higher redshifts. 3σ detections reach $K = 20.6$, which corresponds to an unevolved L^* galaxy at a redshift $z \simeq 2.5$ (for $q_0 = 0.5$). The most important advantage of extending the search to higher redshifts is that at $z \simeq 2.0$ the Lyman α line enters the optical region, and can act as spectral identifier, thus facilitating the redshift determination. This would not only push confirmation of the absorption system/galaxy connection further but also confirm QSO absorption systems as reliable tools for the identification and study of high redshift galaxies.

REFERENCES

Allington-Smith J., Ellis R.S., Zirbel E.L., Oemler A., 1992, *Astrophys. J.*, in press.

Aragón-Salamanca, A., 1991 *Ph.D. Thesis*, Durham University.

Aragón-Salamanca, A., Ellis R.S., Couch W.J., Carter D., 1992, *Mon. Not. R. Astr. Soc.*, in press.

Atwood B., Baldwin J.A., Carswell R.F., 1985, *Astrophys. J.*, **292**, 58.

Babul A., Rees M., 1992, *Preprint.*

Bahcall J.N., Greenstein J.L., Sargent W.L.W., 1968, *Astrophys. J.*, **153**, 689.

Bahcall J.N. and Peebles P.J.E., 1969, *Astrophys. J. Lett.*, **156**, L7.

Bahcall J.N. and Salpeter E.E., 1965, *Astrophys. J.*,**142**, 1677.

Bahcall J.N. and Spitzer, L., 1969, *Astrophys. J. Lett.*, **156**, L63.

Bajtlik S., Duncan R.C., Ostriker J.P., 1988, *Astrophys. J.*, **327**, 570.

Bechtold J., Ellingson E., 1992, *Astrophys. J.*, **396**, 20.

Bergeron J.A., 1986, *Astr. Astrophys. Letters*, **155**, L8.

Bergeron J.A., 1988, in *Large Scale Structures in the Universe, IAU Symposium no. 130*, Eds. Audouze J., Pelletan M.C., Szalay A., p. 343.

Bergeron J.A., Boissé P., 1991, *Astr. Astrophys.*, **243**, 344 (B&B).

Blades J.C., Hunstead R.W., Murdoch H.S., Pettini M., 1982, *Mon. Not. R. Astr. Soc.*, **200**, 1091.

Broadhurst T.J., Ellis R.S., Glazebrook, K., 1992, *Nature*, **355**, 55.

Broadhurst T.J., Ellis R.S., Shanks T., 1988, *Mon. Not. R. Astr. Soc.*, **235**, 827.

Bruzual-A. G., Charlot S., 1992, *preprint.*

Butcher H.R., Oemler A., 1978, *Astrophys. J.*, **219**, 18.

Butcher H.R., Oemler A., 1984, *Astrophys. J.*, **285**, 426.

Buzzoni A., 1989, *Astrophys. J. Suppl.*, **71**, 817.

Carswell R.F., Morton D.C., Smith M.G., Stockton A.N., Turnshek D.A., Weymann R.J., 1984, *Astrophys. J.*, **278**, 486.

Colless M., Ellis R.S., Taylor K., Hook R.N., 1990, *Mon. Not. R. Astr. Soc.*, **244**, 408.

Couch W.J., Ellis R.S., Sharples R.M., Smail I., 1992, *preprint.*

Cowie, L.L., Gardner J.P., Hu E.M., Wainscoat R.J., Hoddapp K.W., 1991a, *preprint.*

Cowie L.L., Gardner J.P., Lilly S.J., McLean I., 1990, *Astrophys. J. Lett.*, **360**, L1.

Cowie L.L., Songaila A., Hu E.M., 1991b, *Nature*, **354**, 460.

Davis M., Efstathiou G., Frenk C.S., White S.D.M., 1985, *Astrophys. J.*, **292**, 371.

de Lapparent V., Geller M.J., Huchra J.P., 1989, *Astrophys. J.*, **343**, 1.

Dressler A., Gunn J.E., 1990, in *Evolution of the Universe of Galaxies, Hubble Symposium*, Ed. Kron R.G., ASP Conference Series, p. 200.

Elias J.H., Frogel J.A., Mathews K., Neubegauer G., 1982, *Astron. J.*, **87**, 1029.

Ellis R.S., 1982, in *The Origin and Evolution of Galaxies*, Eds. Jones B.J.T. & Jones J.E., Dordrecht, Reidel, p. 255.

Ellis R.S., Parry I.R., 1987, in *Instrumentation for Ground-Based Optical Astronomy*, ed. L.B. Robinson, Springer-Verlag, New York, p. 192.

Foltz C.B., Weymann R.J., Peterson B.M., Light Sun, Malkan M.A., Chaffee F.H., 1986, *Astrophys. J.*, **307**, 504.

Glazebrook, K., 1991, *Ph.D. Thesis*, Edinburgh University.

Guiderdoni 1991, in *Observational Tests of Cosmological Inflation*, eds. T. Shanks *et al.*, Kluwer, Dordrecht, p. 217.

Guiderdoni B., Rocca-Volmerange B., 1990, *Astr. Astrophys.*, **227**, 362.

Guth A.H., 1991, in *Observational Tests of Cosmological Inflation*, eds. T. Shanks *et al.*, Kluwer, Dordrecht, p. 1.

Haschick A.D., Burke B.F., 1975, *Astrophys. J. Lett.*, **200**, L137.

Hewitt A., Burbidge G., 1987, *Astrophys. J. Suppl.*, **63**, 1.

Holmberg E., 1976, in *Galaxies and the Universe*, Eds. Sandage A., Sandage M., Kristian J., Univ. of Chicago Press, p. 123.

Kron R.G. 1978, *Ph.D. Thesis*, University of California, Berkeley.

Lanzetta K.M., 1988, *Astrophys. J.*, **332**, 96.

Lehnert M.D., Heckman T.M., Chambers K.C., Miley G.K., 1992, *Astrophys. J.*, **393**, 68.

Lilly S.J., 1988, *Astrophys. J.*, **333**, 161.

Lilly S.J., Cowie L.L., 1986, in *Infrared Astronomy with Arrays*, eds. Wynn-Williams C.G., Becklin E.E., Univ. of Hawaii Institute for Astronomy, p. 473.

Lilly S.J., Cowie L.L., Gardner J.P., 1991, *Astrophys. J.*, **369**, 79.

Loveday J., Peterson B.M., Efstathiou G., Maddox S.J., 1992, *Astrophys. J.*, **390**, 338.

McLean I.S., Chuter T.C., MacCaughrean M.J., Rayner J.T., 1986, *Proc. S.P.I.E*, **627**, 430.

Metcalfe N., Shanks T., Fong R., 1991, *Gemini*, **34**, 12.

Meylan G., Djorgovski S., Weir N., Shaver P., 1990, in *Gravitational Lensing*, eds. Mellier Y. *et al.* , Springer-Verlag, p.111.

Mobasher, B.M., Sharples R.M., Ellis R.S., 1992, *Mon. Not. R. Astr. Soc.*, in press.

Murdoch H.S., Hunstead R.W., Pettini M., Blades J.C., 1986, *Astrophys. J.*, **309**, 19.

Oemler 1992 in *Clusters and Superclusters of Galaxies*, ed. A.C. Fabian, Kluwer, Dordrecht, p. 29.

Peterson B.A., Ellis R.S., Kibblewhite E.J., Bridgeland M.T., Hooley T., Horne D., 1979, *Astrophys. J. Lett.*, **233**, L109.

Phillipps S., Disney M.J., Davies J.I., 1992, *Mon. Not. R. Astr. Soc.*, in press.

Rocca-Volmerange B., Guiderdoni B., 1988, *Astr. Astrophys. Suppl.*, **75**, 93.

Sargent W.L.W., Boksenberg A., Steidel C.C., 1988, *Astrophys. J. Suppl.*, **68**, 539 (SBS).

Sargent W.L.W., Steidel C.C., Boksenberg A., 1988, *Astrophys. J.*, **334**, 22.

Sargent W.L.W., Steidel C.C., Boksenberg A., 1989, *Astrophys. J. Suppl.*, **69**, 703.

Schechter P., 1976, *Astrophys. J.*, **203**, 297.

Steidel C.C., 1990, *Astrophys. J. Suppl.*, **72**,1.

Steidel C.C., 1993a, in *Galaxy Evolution: the Milky Way Perspective*, ASP Conference Series, in press.

Steidel C.C., 1993b, in *The Evolution of Galaxies and their Environments*, eds. Shull J.M., Thronson H., Kluwer, in press.

Steidel C.C., Sargent W.L.W., 1992, *Astrophys. J. Suppl.*, **80**, 1 (SS92).

Tinsley B.M., 1980, *Fundam. Cosmic Physics*, **5**, 287.

Tyson A.J., 1988a, *A.J.*, **96**, 1.

Tyson A.J., 1988b, *Astrophys. J.***335**, 552.

Tyson A.J., Jarvis J.F., 1979, *Ap.J.Letters*, **230**, L153.

Tytler D., Boksenberg A., Sargent W.L.W., Young P., Kunth D., 1987, *Astrophys. J. Suppl.*, **64**, 667.

Wagoner R., 1967, *Astrophys. J.*, **149**, 465.

Weymann R.J., Boroson T.A., Peterson B.M., Butcher H.R., 1978, *Astrophys. J.*, **226**, 603.

Yee H.K.C., 1988, in *Evolution of the Universe of Galaxies, Hubble Symposium*, Ed. Kron R.G., ASP Conference Series, p. 322.

Yee H.K.C., Green R.F., 1987, *Astrophys. J.*, **319**, 28.

York D.G., Yanny B., Crotts A., Carilli C., Garrison E., Matheson L., 1991, *Mon. Not. R. Astr. Soc.*, **250**, 24.

Young P., Sargent W.L.W., Boksenberg A., 1982, *Astrophys. J. Suppl.*, **48**, 455 (YSB).

Zepf S.E., 1991, *Ph.D. Thesis*, John Hopkins University.

APPENDIX: CATALOGUES OF DETECTED SOURCES

Catalogues are presented for the 11 QSO fields analysed in this survey. Each catalogue contains the object's ID, X and Y coordinates in pixels and K magnitude and error. Object number 1 in each field is always the QSO.

Table A1: Q0013−004 Field.

ID	X	Y	K	ΔK
1	29.6	27.4	14.89	0.02
2	21.4	31.8	18.63	0.13
3	45.4	30.7	17.98	0.10
4	33.2	50.7	18.79	0.15
5	19.5	46.3	19.51	0.20
6	16.0	46.0	21.26	0.69
7	38.5	47.3	20.40	0.32
8	31.4	37.3	20.18	0.31
9	52.0	48.0	21.12	0.57
10	46.7	46.2	21.80	0.85
11	-	-	-	-
12	52.9	20.0	19.64	0.22
13	6.42	9.37	16.01	0.04
14	14.4	31.3	20.50	0.34
15	12.4	29.4	20.32	0.33
16	37.6	12.7	20.32	0.32
17	26.7	12.1	20.45	0.40
18	-	-	-	-
19	42.9	7.46	20.81	0.50
20	43.0	16.0	21.36	0.76
21	48.6	11.9	20.99	0.47
22	29.5	24.5	20.32	0.28
23	34.0	27.0	20.21	0.30
24	23.4	34.3	20.20	0.28

Table A2: Q0151+048 Field.

ID	X	Y	K	ΔK
1	31.0	29.0	15.82	0.02
2	29.0	31.0	19.40	0.14
3	28.0	34.0	18.57	0.09
4	34.0	27.0	18.66	0.10
5	32.0	26.0	19.84	0.17
6	17.1	32.2	20.24	0.28
7	16.9	24.2	19.98	0.27
8	24.4	7.9	20.11	0.28
9	56.4	19.4	18.71	0.12
10	52.6	45.0	18.94	0.14
11	54.0	43.0	19.84	0.25
12	24.9	11.9	20.55	0.39
13	18.0	23.0	20.65	0.47
14	29.9	48.9	20.51	0.3
15	21.3	47.3	20.79	0.49
16	-	-	-	-
17	31.0	4.6	20.42	0.38
18	43.6	7.9	20.85	0.49
19	57.5	5.5	20.52	0.42
20	-	-	-	-
21	11.4	46.9	20.96	0.56
22	31.7	43.4	21.63	0.97
23	51.8	34.3	20.79	0.52
24	44.3	33.3	20.31	0.36
25	43.0	43.0	21.18	0.61
26	38.3	48.2	21.47	0.67
27	46.3	49.5	20.66	0 .47
28	28.8	48.5	20.64	0.47
29	-	-	-	-

Table A3: BLL0215+015 Field.

ID	X	Y	K	ΔK
1	29.9	28.9	14.43	0.02
2	30.0	25.0	19.08	0.16
3	33.0	27.0	19.76	0.21
4	29.0	32.0	19.47	0.18
5	22.3	52.1	17.58	0.08
6	18.0	52.0	18.71	0.14
7	14.4	50.2	18.78	0.14
8	17.8	44.3	18.34	0.11
9	20.0	47.0	19.29	0.18
10	14.4	50.2	20.27	0.33
11	9.5	37.0	19.39	0.18
12	10.0	27.9	19.29	0.18
13	-	-	-	-
14	-	-	-	-
15	8.9	6.9	20.11	0.27
16	16.0	9.0	17.60	0.08
17	19.9	6.98	17.23	0.06
18	29.3	12.1	19.37	0.19
19	43.8	11.5	18.81	0.14
20	54.3	7.37	18.97	0.15
21	51.0	17.0	18.39	0.11
22	55.0	18.0	18.25	0.11
23	53.8	26.1	20.99	0.55
24	45.9	23.6	19.84	0.25
25	43.0	21.0	20.01	0.37
26	38.1	21.8	19.39	0.21
27	47.7	36.5	20.01	0.28
28	55.0	40.0	20.55	0.38
29	51.4	42.2	17.67	0.08
30	37.6	40.4	19.29	0.18
31	41.1	45.5	17.18	0.06
32	45.0	44.0	18.17	0.10
33	-	-	-	-
34	46.9	50.6	19.00	0.16
35	19.5	33.2	19.76	0.23

Table A3 (Continued): BLL0215+015 Field.

36	18.0	31.0	20.01	0.30
37	15.0	23.0	24.41	0.40
38	23.5	19.4	19.93	0.31
39	25.0	21.0	20.51	0.51
40	27.0	25.0	20.03	0.31
41	-	-	-	-
42	35	47	21.01	0.51

Table A4: Q0237−233 Field.

ID	X	Y	K	ΔK
1	30.5	31.3	13.71	0.01
2	31.0	28.0	19.31	0.17
3	34.0	30.0	19.03	0.15
4	41.2	35.1	18.71	0.13
5	21.0	22.5	14.74	0.02
6	19.8	32.6	20.00	0.30
7	8.1	36.2	18.82	0.14
8	13.6	39.3	20.22	0.30
9	14.3	39.2	20.68	0.40
10	13.6	39.3	21.42	0.68
11	14.4	13.6	19.49	0.19
16	40.0	10.0	19.46	0.14
17	38.7	12.2	19.22	0.17
18	42.2	16.7	19.62	0.21
19	52.6	17.7	19.04	0.16
21	47.7	10.5	21.21	0.54
24	47.7	25.6	19.85	0.26
27	46.9	41.9	21.32	0.59

Table A5: Q0421+019 Field.

ID	X	Y	K	ΔK
1	31.5	29.5	14.51	0.01
2	34.0	26.0	19.59	0.19
3	35.0	29.0	19.24	0.16
4	31.0	26.0	19.17	0.15
5	36.0	32.0	20.91	0.37
6	37.2	37.4	17.23	0.06
7	43.7	33.4	20.07	0.28
8	48.8	36.5	19.03	0.16
9	54.1	42.6	20.05	0.31
10	44.0	43.0	20.25	0.32
11	48.0	45.0	20.10	0.33
12	46.0	47.0	20.18	0.34
13	38.1	52.6	18.19	0.10
14	35.0	50.0	21.26	0.68
15	22.9	53.0	17.36	0.07
16	16.9	51.0	19.69	0.24
17	14.6	43.4	15.27	0.03
18	10.2	48.6	19.66	0.22
19	-	-	-	-
20	7.7	31.5	19.99	0.31
21	-	-	-	-
22	-	-	-	-
23	-	-	-	-
24	11.2	17.2	20.34	0.32
25	13.0	15.0	21.01	0.56
26	-	-	-	-
27	15.3	5.41	18.06	0.10
28	29.0	10.1	18.20	0.10
29	-	-	-	-
30	36.0	10.0	20.92	0.54
31	41.0	17.0	19.88	0.27
32	55.5	14.3	17.33	0.07
33	38.0	19.0	20.67	0.45
34	-	-	-	-
35	17.0	28.0	20.61	0.41

Table A5 (Continued): Q0421+019 Field.

36	16.5	21.8	21.20	0.63
37	15.0	26.0	20.73	0.44
38	38.0	28.0	20.43	0.30
39	21.2	38.3	19.10	0.16

Table A6: Q0424−130 Field.

ID	X	Y	K	ΔK
1	31.2	27.6	14.34	0.02
2	35.4	30.4	19.80	0.29
3	35.9	27.7	19.50	0.23
4	-	-	-	-
5	25.4	31.1	18.46	0.13
6	32.2	35.5	19.57	0.24
7	37.4	39.6	18.60	0.14
8	42.4	45.4	19.46	0.24
9	33.6	45.6	18.79	0.16
10	29.5	47.1	19.50	0.24
11	21.3	42.5	16.66	0.05
12	7.6	35.3	18.19	0.11
13	-	-	-	-
14	14.4	22.5	20.25	0.39
15	12.0	18.4	20.28	0.39
16	13.5	12.0	21.38	0.96
17	21.9	9.3	19.39	0.22
18	25.2	11.9	18.21	0.11
19	39.5	14.3	19.61	0.24
20	47.3	15.2	20.38	0.41
21	42.4	25.9	19.30	0.20
22	52.0	30.3	19.06	0.18
23	52.2	16.3	19.60	0.24
24	43.4	48.8	20.60	0.58
25	16.1	49.8	20.59	0.59
26	-	-	-	-
27	-	-	-	-
28	35.8	16.5	20.48	0.46
29	18.2	45.6	20.70	0.59

Table A7: Q0836+195 Field.

ID	X	Y	K	ΔK
1	32.1	29.0	15.19	0.02
2	-	-	-	-
3	-	-	-	-
4	-	-	-	-
5	22.4	33.5	19.70	0.22
6	20.9	30.3	19.16	0.16
7	24.0	29.7	20.10	0.25
8	16.2	23.0	20.37	0.31
9	22.1	18.3	20.57	0.42
10	16.2	15.2	20.86	0.51
11	27.0	17.3	19.82	0.25
12	32.1	15.1	17.59	0.07
13	47.4	17.4	19.23	0.17
14	50.5	16.2	18.50	0.12
15	46.1	14.2	21.10	0.58
16	52.1	10.2	18.54	0.12
17	52.2	29.0	20.71	0.41
18	45.1	21.0	21.00	0.52
19	44.1	35.0	20.24	0.31
20	50.2	51.5	16.99	0.06
21	35.8	31.3	20.51	0.36

Table A8: Q0854+191 Field.

ID	X	Y	K	ΔK
1	30.2	30.9	15.52	0.02
2	27.8	32.9	19.90	0.29
3	27.0	30.0	20.60	0.50
4	22.5	38.5	19.46	0.21
5	23.5	50.4	18.85	0.15
6	15.1	51.5	19.09	0.19
7	-	-	-	-
8	12.1	38.4	21.14	0.69
9	17.2	36.1	21.02	0.73
10	19.5	31.4	20.53	0.46
11	18.8	27.7	20.51	0.45
12	15.0	26.1	18.89	0.15
13	8.1	24.3	19.52	0.23
14	-	-	-	-
15	6.5	13.1	19.22	0.18
16	22.2	12.2	19.96	0.29
17	-	-	-	-
18	-	-	-	-
19	24.3	25.6	20.39	0.37
20	29.9	16.2	19.73	0.24
21	31.9	20.9	19.84	0.26
22	29.4	25.9	20.69	0.47
23	38.2	19.1	20.77	0.46
24	36.3	13.5	20.92	0.50
25	34.0	10.1	20.35	0.38
26	42.1	12.3	20.68	0.51
27	45.1	20.2	19.94	0.27
28	-	-	-	-
29	-	-	-	-
30	-	-	-	-
31	-	-	-	-
32	-	-	-	-
33	34.2	37.4	20.54	0.47
34	-	-	-	-
35	-	-	-	-

Table A8 (Continued): Q0854+191 Field.

36	37.5	44.8	20.66	0.48
37	38.8	51.0	20.34	0.37
38	34.8	48.2	20.46	0.42
39	24.9	34.2	20.56	0.50
40	9.2	30.4	20.81	0.54
41	10.2	50.4	19.57	0.23

Table A9: Q1329+412 Field.

ID	X	Y	K	ΔK
1	31.0	28.1	14.88	0.02
2	40.1	41.2	15.00	0.02
3	31.9	41.1	18.73	0.13
4	22.0	37.2	19.25	0.18
5	21.1	40.9	20.18	0.34
6	22.2	44.3	21.62	1.07
7	15.1	34.0	18.91	0.15
8	14.1	23.1	18.23	0.10
9	14.1	9.1	18.36	0.11
10	25.5	9.9	21.24	0.68
11	30.2	15.1	19.35	0.19
12	37.1	15.3	18.80	0.14
13	39.7	17.5	17.95	0.09
14	42.9	14.1	19.17	0.18
15	41.5	9.2	17.72	0.08
16	52.0	11.5	16.22	0.04
17	53.8	19.2	19.31	0.19
18	50.2	21.0	18.76	0.14
19	44.1	21.1	18.17	0.10
20	44.7	23.5	17.78	0.08
21	51.1	26.0	19.58	0.21
22	56.5	32.5	16.44	0.04
23	50.2	40.4	18.81	0.15
24	16.7	12.3	19.95	0.26
25	33.7	29.9	19.75	0.26
26	36.5	33.5	21.19	0.70
27	26.4	25.0	20.68	0.42
28	44.0	43.6	20.43	0.41
29	6.5	22.0	20.28	0.35
30	-	-	-	-
31	-	-	-	-
32	-	-	-	-
33	-	-	-	-
34	-	-	-	-
35	-	-	-	-

Table A9 (Continued): Q1329+412 Field.

ID	X	Y	K	ΔK
36	-	-	-	-
37	54.5	46.2	20.30	0.36
38	-	-	-	-
39	29.3	43.9	20.89	0.57
40	17.2	25.7	20.92	0.54
41	-	-	-	-
42	-	-	-	-
43	7.3	6.0	20.94	0.59
44	27.1	12.9	20.40	0.36
45	48.1	37.3	20.73	0.53

Table A10: Q1331+170 Field.

ID	X	Y	K	ΔK
1	29.8	30.2	13.60	0.01
2	31.5	27.2	18.57	0.12
3	24.4	39.5	19.87	0.24
4	13.5	44.4	20.88	0.53
5	12.6	49.7	19.70	0.26
6	14.9	32.2	21.07	0.48
7	5.7	33.8	21.21	0.60
8	7.5	24.0	17.56	0.07
9	14.6	22.5	18.47	0.12
10	18.3	27.2	19.38	0.18
11	7.6	17.3	21.83	0.90
12	10.0	14.9	18.65	0.13
13	27.7	13.6	21.11	0.56
14	-	-	-	-
15	32.5	15.8	21.65	0.84
16	-	-	-	-
17	-	-	-	-
18	46.8	9.2	17.83	0.08
19	51.4	14.6	20.13	0.27
20	-	-	-	-
21	52.3	22.7	21.83	0.90
22	53.9	24.7	20.44	0.32
23	48.4	25.5	18.97	0.15
24	39.6	25.8	19.49	0.20
25	41.8	22.9	20.94	0.53
26	54.1	41.2	15.36	0.03
27	-	-	-	-
28	-	-	-	-
29	-	-	-	-
30	-	-	-	-
31	33.2	33.6	20.03	0.27
32	11.3	11.9	19.22	0.16

Table A11: Q2044−168 Field.

ID	X	Y	K	ΔK
1	30.6	29.3	15.30	0.03
2	26.4	29.4	17.80	0.08
3	37.6	33.4	20.04	0.35
4	42.0	26.0	20.24	0.32
5	44.1	28.2	19.78	0.26
6	45.0	30.0	20.41	0.34
7	53.3	36.6	20.67	0.42
8	49.1	41.4	20.58	0.43
9	48.0	43.0	20.80	0.48
10	48.6	44.4	20.97	0.55
11	45.0	45.0	21.43	0.79
12	40.8	43.6	18.29	0.11
13	38.0	47.0	20.86	0.59
14	29.8	51.1	19.34	0.20
15	29.6	41.6	20.19	0.37
16	21.3	42.7	16.26	0.04
17	21.4	35.7	19.66	0.23
18	17.0	46.0	20.33	0.36
19	-	-	-	-
20	6.41	44.3	20.80	0.52
21	9.56	31.9	14.67	0.02
22	7.0	29.0	20.12	0.33
23	14.7	24.5	20.15	0.30
24	19.6	23.4	20.72	0.48
25	24.2	22.3	20.24	0.32
26	31.8	17.4	20.06	0.29
27	20.5	8.60	14.57	0.02
28	34.8	9.40	17.52	0.08
29	38.0	11.0	19.32	0.19
30	37.0	13.0	19.40	0.20
31	44.7	15.7	21.26	0.61
32	48.7	10.5	20.56	0.44
33	50.0	8.0	20.86	0.51
34	53.7	8.4	20.44	0.38
35	53.8	16.1	21.08	0.54

Table A11 (Continued): Q2044−168 Field.

36	10.7	10.6	20.30	0.65
37	8.20	17.8	21.30	0.65
38	45.7	24.7	21.60	0.80
39	42.2	21.4	20.02	0.29

ACKNOWLEDGEMENTS

I would like to thank my supervisor, Richard Ellis, for his expert guidance and support during my stay at Durham, as well as for obtaining financial support for an observing trip. Several people in the Physics Department helped me in different ways, either by providing a warm, friendly atmosphere or through expert advice on many different aspects of my work. Special thanks go to Karl Glazebrook for many encouraging comments and useful advice on my thesis. I am grateful to Alfonso Aragón-Salamanca for many fruitful discussions. I am also grateful to all the Starlink staff, particularly Alan Lotts and Nick Eaton, for their friendly and expert advice on computing and related topics.

Finally, I am grateful to my parents and my close friends, in Durham and elsewhere, for their unconditional love and support. It would all have been much harder, if not impossible, without their support.